

Three-dimensional hydrodynamic and sediment transport modeling to test the sediment focusing hypothesis in upland lakes

L. A. Morales-Marin ^{a*}, J. R. French, H. Burningham, R. W. Battarbee

UCL Department of Geography, Environmental Change Research Centre, University College London, London, UK

Abstract

Palaeolimnological studies rely on assumptions regarding the distribution and completeness of lake deposits that are not always fully supported by observations. In particular, the assumption that “focusing” of suspended sediments leads to preferential deposition in the deepest part of a lake is not always justified, especially in upland lakes subject to energetic wind forcing. Few studies have investigated the hydrodynamic controls on lake sediment focusing, especially the importance of wind-driven currents in deep water. We combine a three-dimensional numerical hydrodynamic and suspended sediment model (FVCOM) with a semi-empirical wind wave model to investigate the potential mobility of bottom sediments in a small oligotrophic upland lake (Llyn Conwy, north Wales, UK). Exploratory simulations of wave- and current-generated bottom stress and suspended sediment dynamics confirm the expected importance of wave-generated bottom stresses in shallower waters (< 3 m depth) around the shore. Field survey shows that lake sediments are largely absent from this zone. This is consistent with peripheral wave action as a sediment focusing mechanism. In deeper water, wind-driven currents become the dominant contributor to bottom stress. Strong wind forcing events drive an energetic circulation with peak bottom stresses that intermittently exceed any realistic erosion threshold over a large proportion of the lake at depths far below those at which waves can be effective. The spatial distribution of lake sediments, and the completeness of the sediment record, is thus determined by a complex interaction between wind-driven circulation and bathymetry, rather than by bathymetry alone. Although our sediment dynamics simulations are purely exploratory, the results are consistent with survey results that show a patchy distribution of deep-water accumulation. Some implications of these results for the selection of sediment coring locations and the interpretation of sediment records are considered.

Although lakes are often considered less complex than many other sedimentary environments (e.g., Håkanson 1981; Leeder 1982; Margalef 1983), there is considerable interest in their sediment dynamics on account of the importance of lakes as archives of past environmental conditions (e.g., Håkanson 1984; Stumm 1985; Imberger 1998). Sediment accumulation is driven by a variety of physical, geochemical and biological processes, and the resulting sediment sequences record important information on changing

environmental conditions within lake water bodies (Battarbee 1978) and their catchments (Davis 1969; Foster et al. 1988; Smol 1992), as well as broader scale changes in climate (Fritz 1996; Battarbee 2000; Solovieva et al. 2005; Wang et al. 2008). Sedimentation may be quite rapid, often of the order of a few mm yr⁻¹ (Brothers et al. 2008) and the high preservation potential (Leeder 1982; Verschuren 1999) potentially allows more-or-less continuous reconstruction of environmental changes at decadal resolution or better (e.g., Stern et al. 2005). Many glacial lakes are characterized by annually laminated sediments, which reflect seasonal variation in meltwater and clastic sediment input (Itkonen and Salonen 1994) and provide an absolute incremental chronology (O’Sullivan 1983; Gajewski et al. 1997). Elsewhere, lake sediments tend to be massive and their use for palaeolimnological studies depends on good chronological control, as well as the assumption that the depth of homogenization of the sub-fossil record due to resuspension and vertical mixing is less than the sampling interval (Larsen and MacDonald 1993).

*Correspondence: luis.marin@usask.ca

^aPresent address: Global Institute for Water Security and School of Environment and Sustainability, University of Saskatchewan, Saskatoon, Saskatchewan, Canada

Additional Supporting Information may be found in the online version of this article.

This is an open access article under the terms of the Creative Commons Attribution License, which permits use, distribution and reproduction in any medium, provided the original work is properly cited.

Quantitative analysis of lake sediment accumulation is complicated by the tendency of deposited sediments to be resuspended within shallow marginal areas and transported progressively to deeper waters; Likens and Davis (1975) coined the term “sediment focusing” to describe this set of processes. Gross accumulation rates, as measured by short-term sediment trap deployments, are typically higher in shallow areas as a result of resuspension by waves and currents (Evans 1994). Deeper areas, especially in stratified lakes, are not directly influenced by wave-induced bottom stresses and typically experience less energetic currents (Håkanson 1977; Verschuren 1999) and higher net accumulation rates (Davis 1969).

The work of Hilton (1985) and Hilton et al. (1986a) has been especially valuable in providing a conceptual framework for understanding sedimentation in small lakes. Hilton et al. (1986a) identified 10 distinct mechanisms for sediment dispersal. Four of these are potentially associated with sediment focusing: peripheral wave action; intermittent complete mixing; slumping and sliding; and organic degradation. From a multi-core study of Esthwaite Water, a small eutrophic lake in the English Lake District, they concluded that processes associated with sediment focusing accounted for 59% of the variance in sediment accumulation rate. Of these, peripheral wave action and intermittent complete mixing appeared to be the most important.

The assumption that sediment focusing is the main mechanism controlling the distribution, thickness, and completeness of lake sediment sequences often guides the selection of coring locations in palaeolimnological studies (Dearing 1986; Gilbert 2003). Rowan et al. (1995), for example, present a sampling framework for ^{210}Pb dating based on the mud deposition boundary depth (Rowan et al. 1992). This interprets lake bathymetry to identify erosional, depositional, and transitional zones according to the effectiveness of wave resuspension. Coring can then target the depositional zone. However, sediment accumulation patterns are often more complex than a simple depth-related focusing model implies. In very shallow lakes, extensive areas of the bed may be resuspended by the bottom stress due to wind waves (Blom et al. 1992; Cyr 1998; Kazancı et al. 2010). In deeper lakes, wave re-suspension tends to be restricted to shallow areas around the shoreline and wind-driven currents are more important for sediment dispersal within the main lake basin. At a Holocene time scale, the focus of sedimentation may change as basin infilling alters the water circulation (e.g., Davis and Ford 1982; Blais and Kalff 1995). Although wind-induced currents (Lou et al. 2000) and seicheing (Gloor et al. 1994) are known to influence foci of sedimentation within large lakes, few studies have investigated their efficacy and effect on the preservation potential of deeper water sediment sequences in small lakes. An exception is Odgaard (1993) who used 36 sediment cores to determine the thickness of Holocene sediments in small Danish

lake. A key inference from this unusually intensive study was that wind-driven currents as well as waves exert an important control on the location and thickness of deposits.

Direct observation of sediment exchange between the water column and lake bed is difficult. Trap studies provide insights into cumulative fluxes, but a higher time resolution is needed to resolve wind-driven resuspension that may be very intermittent, especially at greater depths. This favors the use of automated sensors but these are susceptible to long-term calibration drift, and are not always effective at the low suspended sediment concentrations found in many lakes. An alternative is to approach the problem through exploratory modeling to determine the most important controls on sedimentation. One of the few model studies is that by Mackay et al. (2012), who showed that wind-driven currents were sufficient to mobilize small sediment grains at all depths (up to 8.5 m) within Esthwaite Water. However, their study uses a simple analytical relation between wind forcing and the surface current and its decay with depth (Smith 1979).

In this paper, we describe the implementation of a 3D hydrodynamic model and linked wind wave and sediment transport models to more fully investigate the interplay between wind-induced currents and bottom sediment dynamics. An upland lake exposed to energetic wind forcing (Llyn Conwy, Wales, UK) is used as a case study for exploratory modeling of the wind-driven circulation and its likely effect on the distribution and stability of bottom sediments. Aspects of the wind-driven circulation and the surface waves are validated against field observations. The validated hydrodynamic model is used to drive idealized sediment dynamics simulations that examine the potential for sediment resuspension at all locations and depths in the lake. Particular emphasis is placed on the potential for wind-driven currents to resuspend sediment in deeper parts of the lake that would conventionally be assumed to function as sinks for sediment-focusing processes. Some implications of the findings for the selection of coring locations for palaeoenvironmental studies are discussed.

Methods

Case study description

Llyn Conwy (Fig. 1) is a small (40 ha) upland lake situated 450 m above sea level in North Wales, UK (52° 59'56.4" N, 3° 49'8.4" W). The catchment has a maximum elevation of 526 m and a surface geology dominated by Ordovician volcanics and siltstones. Soils are predominantly blanket peats (Patrick and Stevenson 1986) and influxes are dominated by seepage from the peat around the lake shore and direct precipitation. Tiny streams that enter the lake contribute a small fraction of the total water input and even after heavy rainfall are insignificant drivers of the circulation. A single regulated outflow into the River Conwy was inactive during observation periods reported here.

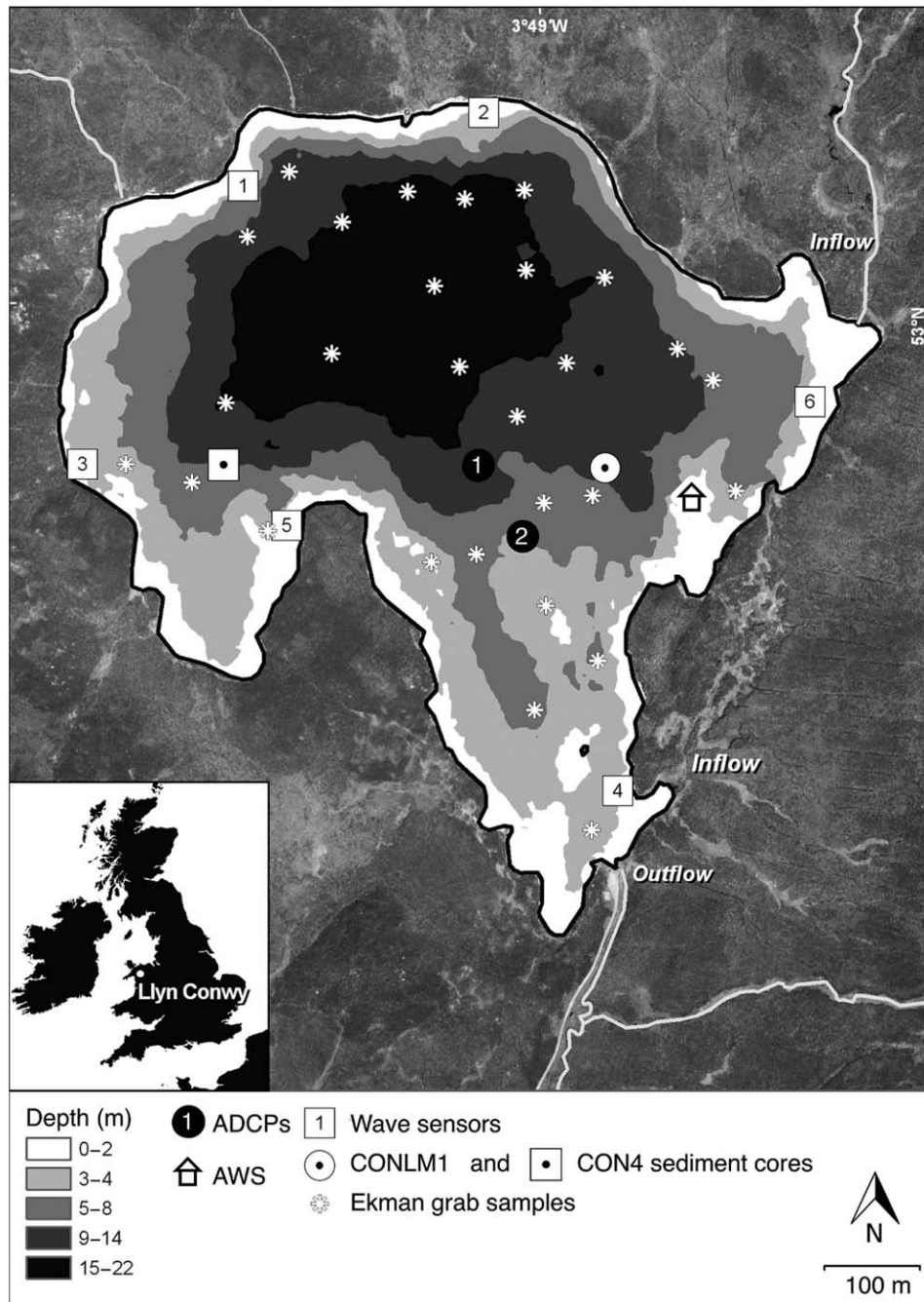


Fig. 1. Llyn Conwy location and composite bathymetry (depth contours in m). Locations of 1987 (CON4) and 2010 (CONLM1) cores and core attempts; Ekman grab samples; ADCPs; wave sensors; and AWS also shown.

Bathymetry is characterized by a central basin with shallower bays to the south and east. Mean and maximum water depth are approximately 7.7 m and 22.0 m. The lake is exposed to predominantly westerly to south-westerly winds. Mean hourly wind speeds are about 10 m s^{-1} and peak hourly wind speeds exceed 30 m s^{-1} (based on analysis of 2006–2008 data from the Centre for Ecology and Hydrology (CEH), Bangor). Mean annual air temperature

and precipitation are approximately 10°C and 2300 mm (Austnes et al. 2010).

Data acquisition

The entire shoreline is characterized by coarse lag gravels and boulders, and a general absence of true lake deposits. Of primary concern in this study are the fine lake muds deposited in deeper water. The extent and composition of these

deposits was investigated using Ekman grab samples that were analyzed for loss on ignition (LOI) at 550°C, water content and grain size. Size analysis was performed using a Malvern MasterSizer 2000 laser granulometer and summary statistics (median diameter (d_{50}) and sorting) determined using Folk and Ward (1957) graphical measures.

The only previous investigation of the sediments at Llyn Conwy has been the acquisition in 1987 of a single core from a depth of 7.4 m on the western margin of the main basin (CON4; Fig. 1). In the present study, an additional core was recovered from a depth of approximately 9 m in the eastern part of the basin (CONLM1; Fig. 1) using a modified rod-less piston corer (Chambers and Cameron 2001) with a 7 cm diameter tube. The 1.2 m core was sliced at 1 cm intervals prior to determinations of bulk density, grain size and LOI. Sub-samples were analyzed for ^{210}Pb , ^{226}Ra , ^{137}Cs , and ^{241}Am by direct gamma assay in the UCL Bloomsbury Environmental Isotope Facility. Analysis was carried out using an ORTEC HPGe GWL series well-type coaxial low background intrinsic germanium detector. ^{210}Pb was determined via gamma emissions at 46.5 keV and ^{226}Ra by the 295 keV and 352 keV gamma rays emitted by its daughter isotope ^{214}Pb following 3 weeks storage in sealed containers to allow radioactive equilibration. ^{137}Cs and ^{241}Am were measured by their emissions at 662 keV and 59.5 keV (Appleby et al. 1986). Absolute efficiencies of the detector were determined using calibrated sources and sediment samples of known activity, and corrections made for the effect of within-sample self absorption of low energy gamma rays (Appleby et al. 1992).

Hydrodynamic modeling is critically dependent on the quality of the bathymetry data (Cea and French 2012). The earlier survey of Patrick and Stevenson (1986) was therefore supplemented using a dGPS-equipped Raytheon sounding system, especially to improve resolution in the shallower bays.

Two field campaigns were undertaken in July 2010 and April 2011 to acquire data to calibrate and validate the 3D hydrodynamic model and validate a fetch-based wind wave model. Vertical velocity profiles were obtained at two locations using a bottom-mounted RDI 1200KHz Workhorse Sentinel Acoustic Doppler Current Profiler (ADCP 1 and 2 in Fig. 1). The ADCP was set to record 3D velocities at a vertical interval of 0.5 m, using ensembles of 150 pings to give a precision (standard deviation) of $\pm 0.057 \text{ m s}^{-1}$. Wind wave measurements were undertaken at six locations around the lake (W1–W6 in Fig. 1) using atmospherically vented Druck PTX1830 pressure sensors sampled at 8 Hz using Campbell CR10 data recorders onshore. Technical problems prevented data capture at W1 and W2. Data blocks of 4096 near-bed pressure readings were used to construct wave height parameters at the free surface (Lee and Wang 1984).

Meteorological data were obtained using a Davis Automatic Weather Station (AWS) equipped with sensors for

wind speed ($\pm 3\%$ accuracy), direction ($\pm 7^\circ$ accuracy), air temperature (accuracy $\pm 1^\circ\text{C}$), pressure (accuracy $\pm 1 \text{ mB}$), and relative humidity (accuracy $\pm 3\%$). The AWS was installed on an islet off the eastern shore of the lake (AWS in Fig. 1), with the sensors 2 m above the water level. An additional AWS record from a data buoy maintained by CEH (Bangor) between 2006 and 2008 was also acquired, together with a 20 yr wind record for Capel Curig (UK Meteorological Office station 1171), 13 km northwest of Llyn Conwy. The Capel Curig data were empirically corrected with reference to the Llyn Conwy AWS data to take account of differences in location and altitude, to allow a more complete analysis of the wind climate.

Computational modeling

FVCOM, an open-source 3D finite-volume model developed originally for ocean applications (Chen et al. 2004, 2011), was used to represent the wind-driven circulation. The equations of mass, momentum, and temperature conservation, cast in a bottom following σ -coordinate system, are given as:

$$\frac{\partial \zeta}{\partial t} + \frac{\partial Du}{\partial y} + \frac{\partial Dv}{\partial y} + \frac{\partial \omega}{\partial \sigma} = 0 \quad (1)$$

$$\begin{aligned} \frac{\partial uD}{\partial t} + \frac{\partial u^2D}{\partial x} + \frac{\partial uvD}{\partial y} + \frac{\partial u\omega D}{\partial \sigma} - f v D = \\ -gD \frac{\partial \zeta}{\partial x} - \frac{gD}{\rho_0} \left[\frac{\partial}{\partial x} \left(D \int_{\sigma}^0 \rho d\sigma' \right) + \sigma \rho \frac{\partial D}{\partial x} \right] + \frac{1}{D} \frac{\partial}{\partial \sigma} \left(K_m \frac{\partial u}{\partial \sigma} \right) + DF_x \end{aligned} \quad (2)$$

$$\begin{aligned} \frac{\partial vD}{\partial t} + \frac{\partial v^2D}{\partial y} + \frac{\partial uvD}{\partial x} + \frac{\partial v\omega D}{\partial \sigma} - f u D = \\ -gD \frac{\partial \zeta}{\partial y} - \frac{gD}{\rho_0} \left[\frac{\partial}{\partial y} \left(D \int_{\sigma}^0 \rho d\sigma' \right) + \sigma \rho \frac{\partial D}{\partial y} \right] + \frac{1}{D} \frac{\partial}{\partial \sigma} \left(K_m \frac{\partial v}{\partial \sigma} \right) + DF_y \end{aligned} \quad (3)$$

$$\frac{\partial TD}{\partial t} + \frac{\partial TuD}{\partial x} + \frac{\partial TvD}{\partial y} + \frac{\partial T\omega D}{\partial \sigma} = \frac{1}{D} \frac{\partial}{\partial \sigma} \left(K_h \frac{\partial T}{\partial \sigma} \right) + D\hat{H} + DF_T \quad (4)$$

$$\rho = \rho(T) \quad (5)$$

where in the horizontal diffusion terms are defined as:

$$DF_x \approx \frac{\partial}{\partial x} \left[2A_m H \frac{\partial u}{\partial x} \right] + \frac{\partial}{\partial y} \left[A_m H \left(\frac{\partial u}{\partial x} + \frac{\partial v}{\partial y} \right) \right] \quad (6)$$

$$DF_y \approx \frac{\partial}{\partial x} \left[A_m H \left(\frac{\partial u}{\partial x} + \frac{\partial v}{\partial y} \right) \right] + \frac{\partial}{\partial y} \left[2A_m H \frac{\partial v}{\partial y} \right] \quad (7)$$

$$DF_T \approx \frac{\partial}{\partial x} \left(A_h H \frac{\partial T}{\partial x} \right) + \frac{\partial}{\partial y} \left(A_h H \frac{\partial T}{\partial y} \right) \quad (8)$$

where u , v , and ω are the velocity components in x , y , and σ directions respectively; T is the water temperature; ρ is the density; f is the Coriolis parameter; K_m is the vertical eddy viscosity coefficient; K_h is the thermal vertical eddy diffusion coefficient; A_m and A_h are the horizontal eddy and thermal

diffusion coefficients, respectively. K_m and K_h are parameterized using the Mellor and Yamada (1982) MY2.5 turbulence closure scheme, as modified by Galperin et al. (1988). A_m and A_h are specified using the Smagorinsky parameterization (Smagorinsky 1963).

The boundary conditions for u , v , ω , and T at the water surface ($\sigma = 0$) are defined as:

$$\left(\frac{\partial u}{\partial x}, \frac{\partial v}{\partial \sigma}\right) = \frac{D}{\rho_o K_m} (\tau_{sx}, \tau_{sy}); \omega = \frac{\hat{E} - \hat{P}}{\rho} \quad (9)$$

$$\frac{\partial T}{\partial \sigma} = \frac{D}{\rho c_p K_h} (Q_n(x, y, t) - SW(x, y, 0, t)) \quad (10)$$

and at the bottom ($\sigma = -1$) as:

$$\left(\frac{\partial u}{\partial \sigma}, \frac{\partial v}{\partial \sigma}\right) = \frac{D}{\rho_o K_m} (\tau_{bx}, \tau_{by}); \omega = \frac{Q_b}{\Omega} \quad (11)$$

$$\frac{\partial T}{\partial \sigma} = \frac{A_h D \tan \alpha}{K_h - A_h \tan^2 \alpha} \frac{\partial T}{\partial n} \quad (12)$$

where \hat{P} and \hat{E} are the precipitation and evaporation rates, respectively; Q_n is the surface net heat flux; $SW(x, y, 0, t)$ is the shortwave flux incident at the water surface; Q_b is the groundwater volume flux at the bottom; Ω is the area of the groundwater source; c_p is the specific heat of water; α is the bottom slope; and n is a horizontal axis.

Following Trenberth (1989), the shear stresses at the water surface are expressed as:

$$\begin{pmatrix} \tau_{sx} \\ \tau_{sy} \end{pmatrix} = \rho_a C_{dw} \begin{pmatrix} w_x \\ w_y \end{pmatrix} \sqrt{w_x^2 + w_y^2} \quad (13)$$

where w_x , w_y are the wind velocity components in x and y respectively, ρ_a is the air density, and C_{dw} is a drag coefficient. There is considerable scatter in experimental determinations of C_{dw} (Yelland and Taylor 1996) and it also has some dependence on wind speed. FVCOM implements this as a constant term (Chen et al. 2011) and we use a value of $C_{dw} = 0.0025$, appropriate to higher windspeeds.

The shear stresses at the bed due to currents are expressed as:

$$\begin{pmatrix} \tau_{cx} \\ \tau_{cy} \end{pmatrix} = \rho C_d \begin{pmatrix} u \\ v \end{pmatrix} \sqrt{u^2 + v^2} \quad (14)$$

where C_d is a drag coefficient determined by matching a logarithmic bottom layer to the model at a height z_{ab} above the bottom; that is:

$$C_d = \max \left[\frac{\kappa^2}{\ln^2 \left(\frac{z_{ab}}{z_o} \right)}, 0.0025 \right] \quad (15)$$

where $\kappa = 0.4$ is the Von Karman constant and z_o is the bottom roughness parameter.

FVCOM models the transport of user-defined size classes of cohesive and non-cohesive material. Each class has fixed attributes of grain diameter, density, settling velocity, critical shear stress for erosion, and erodability constant (Warner et al. 2008; Chen et al. 2011). The suspended load model is represented by the diffusion-advection equation:

$$\begin{aligned} \frac{\partial C_i}{\partial t} + \frac{\partial u C_i}{\partial x} + \frac{\partial v C_i}{\partial y} + \frac{\partial C_i (w - w_i)}{\partial z} &= \frac{\partial}{\partial x} \left(A_h \frac{\partial C_i}{\partial x} \right) + \frac{\partial}{\partial y} \left(A_h \frac{\partial C_i}{\partial y} \right) \\ &+ \frac{\partial}{\partial z} \left(A_h \frac{\partial C_i}{\partial z} \right) \end{aligned} \quad (16)$$

where x , y , and z are the Cartesian coordinates; the sub-indices i represent the sediment class; w_i the settling velocity; and C_i the sediment concentration.

The boundary conditions at the water surface and bed respectively are:

$$K_h \frac{\partial C_i}{\partial z} = 0 \quad (17)$$

$$K_h \frac{\partial C_i}{\partial z} = E_i - D_i \quad (18)$$

Here, D_i is the depositional flux and the erosion rate (E_i) is calculated as:

$$E_i = \delta t Q_i (1 - P_b) f_{bi} \left(\frac{\tau_b}{\tau_{criti}} - 1 \right) \quad (19)$$

where Q_i is the erosive flux, P_b the bottom porosity, f_{bi} the fraction of sediment i in the bed, τ_b the bed shear stress, and τ_{criti} the critical shear stress for erosion of sediment class i .

FVCOM represents the sediment bed as discrete layers initialized with a thickness, sediment-class distribution, porosity, and age. At the beginning of each step, an active layer thickness is calculated based on the relation of Harris and Wiberg (1997),

$$z_a = \max[k_1 (\tau_b - \overline{\tau_{crit}}) \rho_o, 0] + k_2 d_{50} \quad (20)$$

where $\overline{\tau_{crit}}$ is the critical stress for erosion averaged over all sediment classes; d_{50} the median grain size at the surface and k_1 and k_2 are empirical constants (set to 0.007 and 6.0, respectively). The exploratory modeling undertaken in the present study considers only one class of sediment size fraction within a single active layer to understand the potential for currents within the deeper parts of the lake to resuspend unconsolidated material at the bed.

FVCOM can be coupled with a spectral wave model but this significantly increases computational effort for time-dependent problems. To provide a more efficient means of representing bottom stresses due to wind-waves and defining the limit of the mud deposition zone, a new parameterized fetch-limited wind wave model, *UCL-SWM*, was developed (Morales-Marin 2013), based on linear wave theory and

empirical relationships between the wave properties, wind speed, fetch and depth (CERC 1984; Young and Verhagen 1996). *UCL-SWM* estimates wave height, period and frequency, and computes the bottom shear stress due to waves at each node of the *FVCOM* mesh. Within fetch-limited settings, the accuracy of *UCL-SWM*-estimated wave heights is comparable to the more sophisticated *SWAN* spectral wave model (Booij et al. 1999), with both giving errors in wave height < 10%. However, *UCL-SWM* offers an order of magnitude improvement in computational efficiency (Morales-Marin 2013).

UCL-SWM relates non-dimensional wave energy $\epsilon = g^2 E / U_{10}^4$ and non-dimensional peak frequency $\nu = f U_{10} / g$ to the non-dimensional fetch $\chi = g x / U_{10}^2$ and non-dimensional water depth $\delta = g \bar{d} / U_{10}^2$ via the empirical expressions:

$$\epsilon = \alpha_1 \left[\tanh A_1 \tanh \left(\frac{B_1}{\tanh A_1} \right) \right]^{\gamma_1} \quad (21)$$

and

$$\nu = \alpha_2 \left[\tanh A_2 \tanh \left(\frac{B_2}{\tanh A_2} \right) \right]^{\gamma_2} \quad (22)$$

where g is the gravitational acceleration, E is wave energy, f is wave frequency, U_{10} is the wind velocity at an elevation of 10 m given by the expression $U_{10}/U = (10/z)^{1/7}$, x is fetch described as the distance between the point of computation and the upwind shoreline, $A_1 = 0.493 \delta^{0.75}$, $B_1 = 3.13E - 10 \chi^{0.57}$, $A_2 = 0.331 \delta^{1.01}$, $B_2 = 5.215E - 4 \chi^{0.73}$ and the following are calibration constants (Morales-Marin 2013): $\alpha_1 = 8.3E-3$, $\gamma_1 = 1.74$, $\alpha_2 = 0.154$, $\gamma_2 = -0.37$. The value of \bar{d} is calculated as the mean of the water depth along fetch as:

$$\bar{d} = \frac{1}{x} \int_0^x d(x) dx \quad (23)$$

Significant wave height, H , is calculated from $E = \rho g H^2 / 8$ and wave period, T , from $T = U / g \nu$.

Following Dyer (1986), the bottom stress due to waves ($\bar{\tau}_w$) can be given by:

$$\begin{pmatrix} \tau_{wx} \\ \tau_{cy} \end{pmatrix} = \frac{1}{2} \rho f_w \begin{pmatrix} u_{bx} \\ u_{by} \end{pmatrix} \sqrt{u_{bx}^2 + u_{by}^2} \quad (24)$$

where f_w is the friction factor, estimated as:

$$f_w = 2(Re_w)^{-1/2} \quad (25)$$

where $Re_w = U_b A_b / \nu$ is the wave Reynolds Number. Wave orbital velocity, U_b , and wave orbital amplitude, A_b , are estimated using the equations of Luettich et al. (1990) and Ji (2008):

$$U_b = \frac{2\pi H}{T \sinh(k\bar{d})} \quad (26)$$

$$A_b = \frac{U_b T}{2\pi} \quad (27)$$

where k is the wave number obtained implicitly from

$$\frac{2\pi}{T} = \sqrt{gk \tanh(k\bar{d})}. \quad (28)$$

FVCOM and *UCL-SWM* were implemented using an unstructured triangular discretization with 2028 elements (mean length = 13 m) and 12 sigma layers in the vertical. *FVCOM* was calibrated by adjusting the bottom roughness coefficient z_o to obtain the best fit with observed velocity magnitude time series from ADCP-1. Initial conditions were zero velocity throughout the domain and a uniform temperature of 4.71°C, guided by analysis of hourly thermistor string data for 2006–2008 (which showed that the lake stays mixed more than 40% of the time and that even in intermittent stratified periods, the thermocline is weak). Further validation was undertaken with reference to observed velocity profiles from ADCP-2. The *UCL-SWM* wind wave model was validated against wave heights and periods computed from the near-bed pressure datasets.

No data exist with which to quantify sediment inputs into Llyn Conwy. The small inflow streams conveyed no visible plumes of suspended material even after moderate rainfall. Channels cut to drain the upland peat in the mid-20th century have now been blocked up (Patrick and Stevenson 1986) and contemporary input now largely reduced to seepage from the peat and erosion of peat outcrops around the shoreline. Given the diffuse nature of the input, and the primary focus on the extent to which resuspension of existing deep water deposits is possible during windy conditions, sediment sources were neglected.

Model runs

Exploratory sediment dynamics model runs were forced with hourly wind data for December 1997 (Fig. 2). This dataset was chosen to be representative of extreme wind forcing on account of its high mean wind speed (13.4 m s⁻¹) and the occurrence of the highest hourly wind speed recorded between August 1993 and August 2011 (39.5 m s⁻¹). Hourly wind data were re-sampled to the model time-step of 1 s, which was necessary to avoid numerical instabilities at wind speeds > 30 m s⁻¹.

Values for the critical stresses for erosion (τ_{crit}) and deposition (τ_{critd}); the erosion rate constant (δ_E) and porosity (P_o) were obtained from a synthesis of the literature (including Sheng and Lick 1979; Bengtsson and Hellström 1992; Chao et al. 2008). Model output included hourly values of suspended sediment concentration (SSC) at every location within the computational mesh, and the net erosion or deposition at every location at the bed.

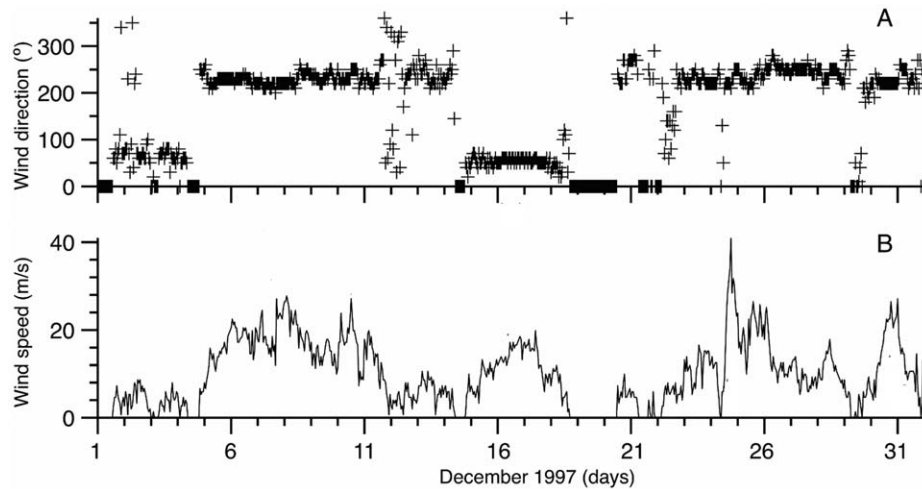


Fig. 2. (A) Hourly wind direction and (B) wind speed for December 1997, based on UK Meteorological Office MIDAS data for Capel Curig, empirically adjusted for Llyn Conwy with reference to CEFAS AWS data for 2006–2008.

Table 1 summarizes the parameter values and the sediment model runs undertaken. Two simulations using the December 1997 meteorological data (runs S1 and S2) investigate spatial patterns of erosion and deposition under transport (infinite active layer thickness) and supply-limited (finite active layer thickness) conditions. A second set of idealized simulations uses the same wind speed time series but applies different constant directions to examine the effect of wind direction on current-generated bottom stress and the implied bed sediment dynamics (runs S3 through S11). A final set of runs explores the sensitivity to the suspended and bed sediment parameters in the combined current and wave model (runs S12 through S20).

Results

Lake bottom sediments

The Ekman grab campaigns resulted in sample recovery from 25 locations, with three returning no sediment. Bottom sediments fall into three distinct types: (1) highly organic lake muds composed of largely of poorly consolidated peat fragments; (2) clay- and silt-rich organic lake muds; and (3) pre-Holocene (i.e., non-lacustrine) buff colored clay and silt with a variable fine gravel fraction. In a few locations, notably in the north-eastern part of the basin, a sparse cover of fine pebbles of compacted peat (mean diameter ≈ 5 mm) were observed overlying pre-Holocene deposits. Along the north shore and in parts of the deep central basin, no sediment was recovered, implying the absence of any Holocene lake sedimentation. Figure 3A summarizes the distribution of these sediment types. While wave-induced bottom stresses clearly preclude fine sedimentation in many shallow marginal areas, it is notable that deeper parts of the basin that lie well below the wave base (the depth at which wave orbital velocities become insignificant, approximated as half

of the wave length; Reading and Collinson 1996) also lack sediments. These areas do not all correspond to steep bottom slopes, implying a hydrodynamic rather than topographic control on sediment accumulation.

As Fig. 3B shows, sediment water content is greater within the mud-dominated western and southern parts of the basin ($W_w > 75\%$) than in the central and eastern areas floored by pre-Holocene clays ($W_w < 45\%$). LOI, used as a proxy for organic matter content, shows a more heterogeneous distribution (Fig. 3C). The highest LOI ($> 60\%$) occurs where peat deposits have been laid down within sheltered shallow water at the southern tip of the lake. More generally, lake muds are characterized by $20 < \text{LOI} < 60\%$. Where pre-Holocene clays persist on the bed, $\text{LOI} < 20\%$. More organic sediments tend also to have high porosity (Håkanson and Jansson 1983) and there is a strong correspondence between LOI and W_w ($r = 0.85$; $n = 25$, $p = 0.02$).

Grain size analysis of mechanically resuspended bottom samples (Fig. 3D; Supporting Information Table 1s) yielded mean d_{50} values of $91.3 \mu\text{m}$, $146.9 \mu\text{m}$, and $40.2 \mu\text{m}$ for organic, clay/silt-rich and pre-Holocene deposits respectively. The first two classes were poorly sorted and the last very poorly sorted. Ultrasonic treatment improved the sorting and reduced the d_{50} to $21.9 \mu\text{m}$, $26.0 \mu\text{m}$, and $14.7 \mu\text{m}$ for the organic, clay/silt-rich and pre-Holocene deposits, respectively, attributable to the breakdown of large peat fragments and composite particles.

Sediment particle densities, ρ_s estimated using the density bottle technique (Hilton et al. 1986b) on raw sediment samples were used in conjunction with the Stokes settling law to estimate settling velocity, w_s (Supporting Information Table 1s). This assumes spherical particles, which is hard to justify given the fibrous nature of the organic fraction. However, these calculations provide a first approximation of the likely

Table 1. Summary of sediment dynamics simulations and parameter values (see text for further explanation of parameters).

	d_{50} mm	ρ_s kg m ⁻³	w_s mm s ⁻¹	δ_E kg m ⁻² s ⁻¹	τ_{crit} Nm ⁻²	τ_{critd} Nm ⁻²	P_o
<i>Currents + waves Dec 1997 wind</i>							
S1	0.091	1700	0.2	2×10^{-5}	0.10	0.08	0.76
S2	0.091	1700	0.2	2×10^{-5}	0.10	0.08	0.76
<i>Currents only Dec 1997 wind, with direction held constant</i>							
S3 actual directions	0.091	1700	0.2	2×10^{-5}	0.10	0.08	0.76
S4 0° wind direction	0.091	1700	0.2	2×10^{-5}	0.10	0.08	0.76
S5 45° direction	0.091	1700	0.2	2×10^{-5}	0.10	0.08	0.76
S6 90° direction	0.091	1700	0.2	2×10^{-5}	0.10	0.08	0.76
S7 135° direction	0.091	1700	0.2	2×10^{-5}	0.10	0.08	0.76
S8 180° direction	0.091	1700	0.2	2×10^{-5}	0.10	0.08	0.76
S9 225° direction	0.091	1700	0.2	2×10^{-5}	0.10	0.08	0.76
S10 270° direction	0.091	1700	0.2	2×10^{-5}	0.10	0.08	0.76
S11 315° direction	0.091	1700	0.2	2×10^{-5}	0.10	0.08	0.76
<i>Currents and waves: parameter sensitivity Dec 1997 wind</i>							
S12	0.091	1700	0.2	2×10^{-5}	0.05	0.04	0.76
S13	0.091	1700	0.2	2×10^{-5}	0.10	0.08	0.76
S14	0.091	1700	0.2	2×10^{-5}	0.20	0.16	0.76
S15	0.022	1850	0.015	2×10^{-5}	0.05	0.04	0.76
S16	0.022	1850	0.015	2×10^{-5}	0.10	0.08	0.76
S17	0.022	1850	0.015	2×10^{-5}	0.20	0.16	0.76
S18	0.091	1850	0.3	2×10^{-5}	0.05	0.04	0.76
S19	0.091	1850	0.3	2×10^{-5}	0.10	0.08	0.76
S20	0.091	1850	0.3	2×10^{-5}	0.20	0.16	0.76

setting behavior for modeling purposes. A value of $w_s = 2 \text{ mm s}^{-1}$ was used for the initial sediment dynamics simulations (S1 and S2, and S3 through S11; Table 1). This corresponds to the d_{50} of the mechanically resuspended organic lake mud deposits. Sensitivity analysis (runs S12 through S20) included the effect of using lower values of d_{50} down to the $22 \text{ }\mu\text{m}$ produced by ultrasonic pre-treatment ($w_s = 0.15 \text{ mm s}^{-1}$).

Historical sedimentation

Radiometric dating of the upper 0.40 m of the CONLM1 sediment core is summarized in Supporting Information Table 2s. Total ^{210}Pb activity reaches equilibrium with supported ^{210}Pb at a depth of 0.27 m. Unsupported ^{210}Pb activities calculated by subtracting supported from total ^{210}Pb activity decline irregularly with depth, which implies that the sedimentation rate has varied over time. The inventory of unsupported ^{210}Pb indicates a mean flux to the core location of $31 \text{ Bq m}^{-2} \text{ yr}^{-1}$. This is lower than the atmospheric ^{210}Pb deposition flux for this region, implying that the core site has experienced a degree of sediment focusing (i.e., preferential deposition).

^{137}Cs activity shows a significant peak at the sediment surface and a down-profile tail of declining activity. ^{241}Am activity also peaks at the surface but is otherwise below the

limit of detection. Both ^{137}Cs and ^{241}Am fallout from atmospheric nuclear testing peaked around 1963. Unlike ^{137}Cs , ^{241}Am is considered to be essentially immobile in vertical sediment sequences (Appleby et al. 1991) and thus provides an unambiguous 1963 marker. The presence of both ^{137}Cs and ^{241}Am activity peaks at the surface suggests that the very top of the profile is missing. Although it is possible that the top of the sediment sequence was lost during coring, the core was acquired and extruded with care and with a seemingly intact sediment–water interface. Alternatively, there may be a virtual cessation of sedimentation since the mid-1960s or, more likely, several centimeters of surface mud have been lost or re-mixed through post-depositional processes.

The CONLM1 chronology suggests an average post 1836 rate of sediment accumulation of $0.0063 \text{ g cm}^{-2} \text{ yr}^{-1}$ or 0.22 cm yr^{-1} . As Fig. 4 shows, sedimentation appears to increase significantly in the 1940s and 1950s, most likely due to enhanced erosion within the catchment (Patrick and Stevenson 1986). The CON4 core shows a similar mean sedimentation rate of 0.28 cm yr^{-1} with a longer phase of increased sedimentation that declines through the 1960s, with minor peaks into the 1980s. The basal rate is averaged between 1900 and 1827. At 0.21 cm yr^{-1} , this is rather higher than the rates for the same period in the CONLM1

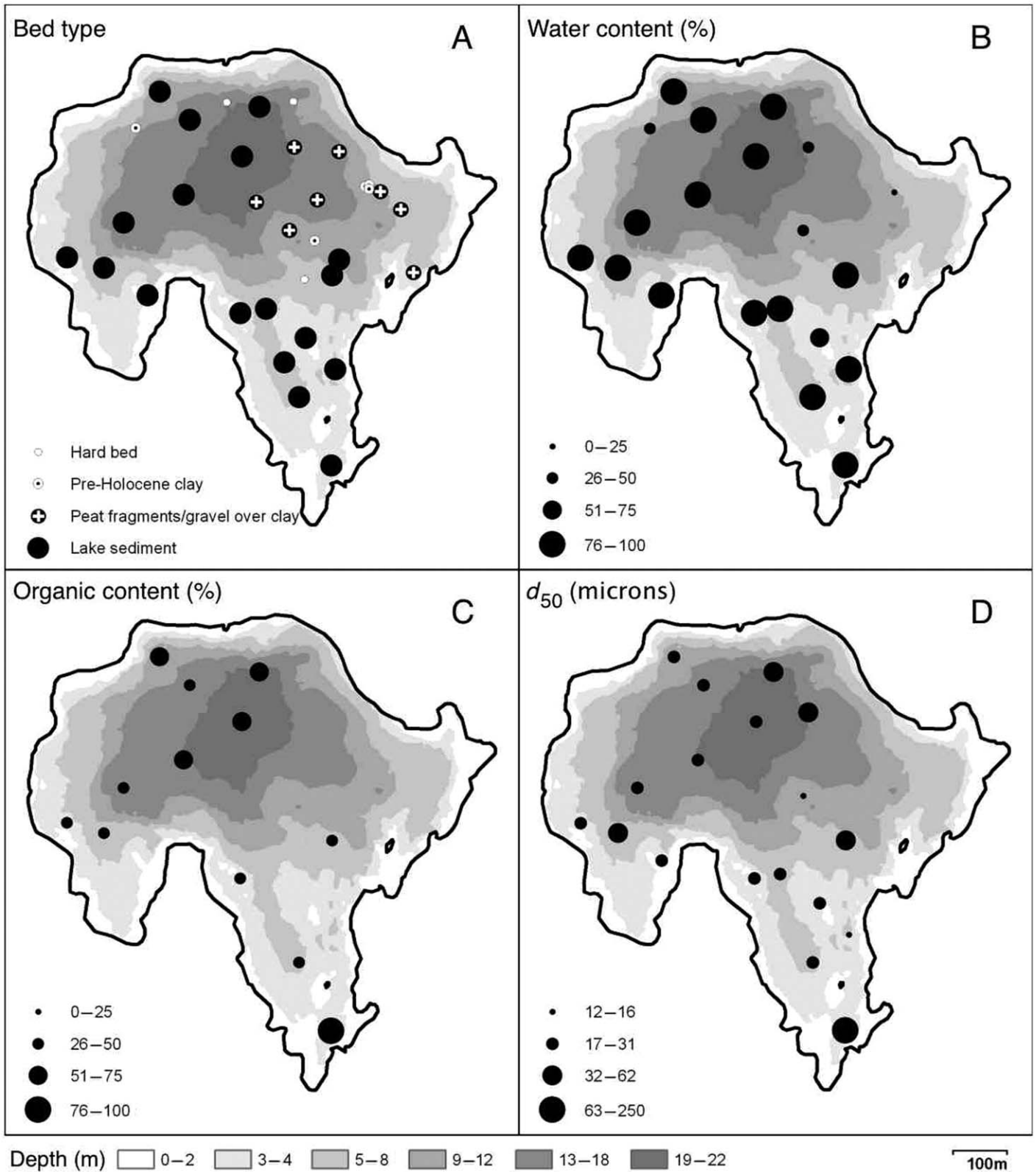


Fig. 3. (A) Classification of bottom sediment type based on Ekman grab returns; (B) sediment water content; (C) LOI (lake muds only); and (D) d_{50} .

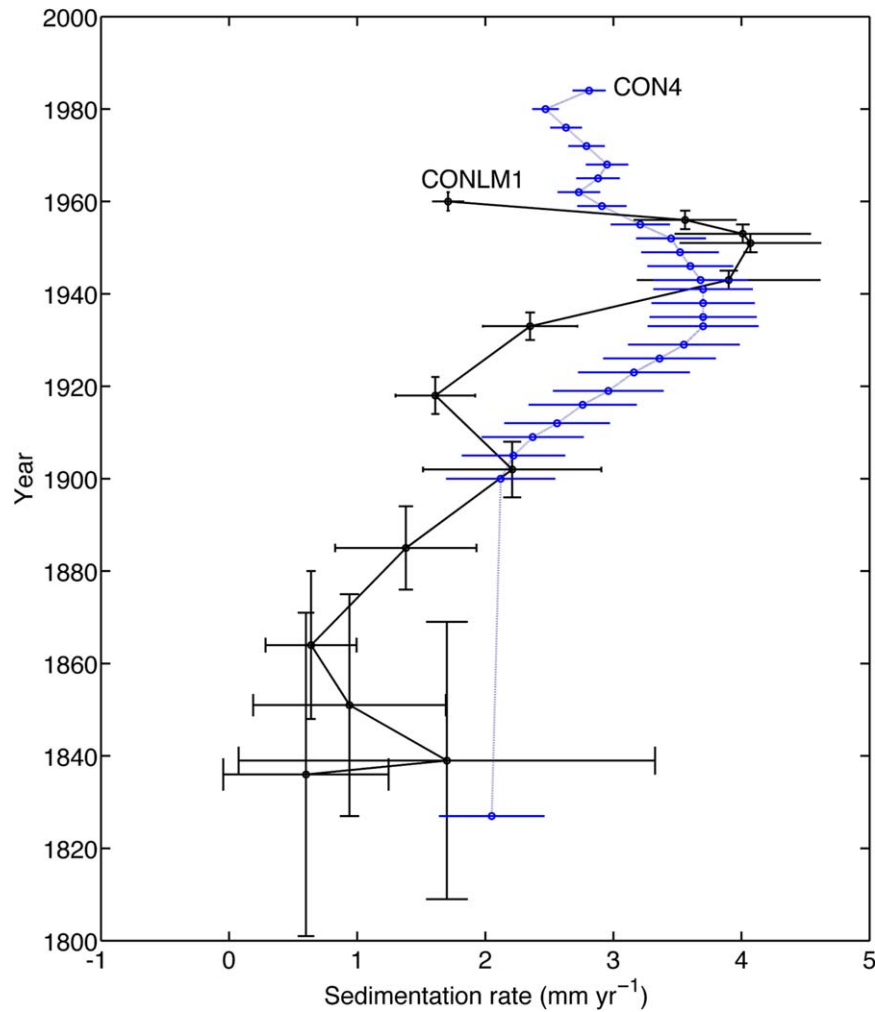


Fig. 4. Sedimentation rate comparison between cores CON4 and CONLM1. Note that CON4 data are averaged for the period 1827–1900. [Color figure can be viewed at wileyonlinelibrary.com]

core. While it is difficult to compare these curves directly, it is tempting to interpret the distinct 1840, 1900, and 1950 maxima and deep intervening minima at CONLM1 as evidence of a site generally conducive to sedimentation but also subject to intermittent reworking under extreme wind forcing events. Removal of poorly consolidated material at the water–sediment interface would introduce step-like discontinuities in the age vs. sedimentation curve. A key question to be investigated through exploratory sediment dynamics modeling is whether such intermittent resuspension is plausible at the CONLM1 site in 9 m of water.

Hydrodynamic model calibration and validation

Comparison of observed and modeled velocity magnitudes at the surface and near the bed showed generally good model performance (Supporting Information Fig. 1s). Nash-Sutcliffe Efficiency (Nash and Sutcliffe 1970) (NSE) scores for the optimal value of $z_o = 0.0277$ m were 0.82 at the surface

and 0.67 near the bed. Both observed and modeled velocity profiles (Supporting Information Fig. 2s) at times with strong wind forcing showed a more-or-less easterly surface current with a westward return flow at depth and a generally good correspondence between modeled and ADCP profiles.

In spite of its assumption of uni-directional propagation of waves and lack of wave diffraction and refraction, validation of *UCL-SWM*, against wind wave observations yielded good performance for H at all stations. Supporting Information Figure 3s shows modeled and observed significant wave height, H , for stations 3 (NSE = 0.81), 4 (NSE = 0.48), 5 (NSE = 0.75), and 6 (NSE = 0.74). Strong correlations ($r > 0.70$) between observed and simulated H and T further demonstrate the ability of this semi-empirical model to estimate spatial and temporal variation in wind wave characteristics. There is some under-estimation of both wave heights (Supporting Information Fig. 3s) and surface currents (Supporting Information Fig. 1s) on Day 5. The fact that both are under-

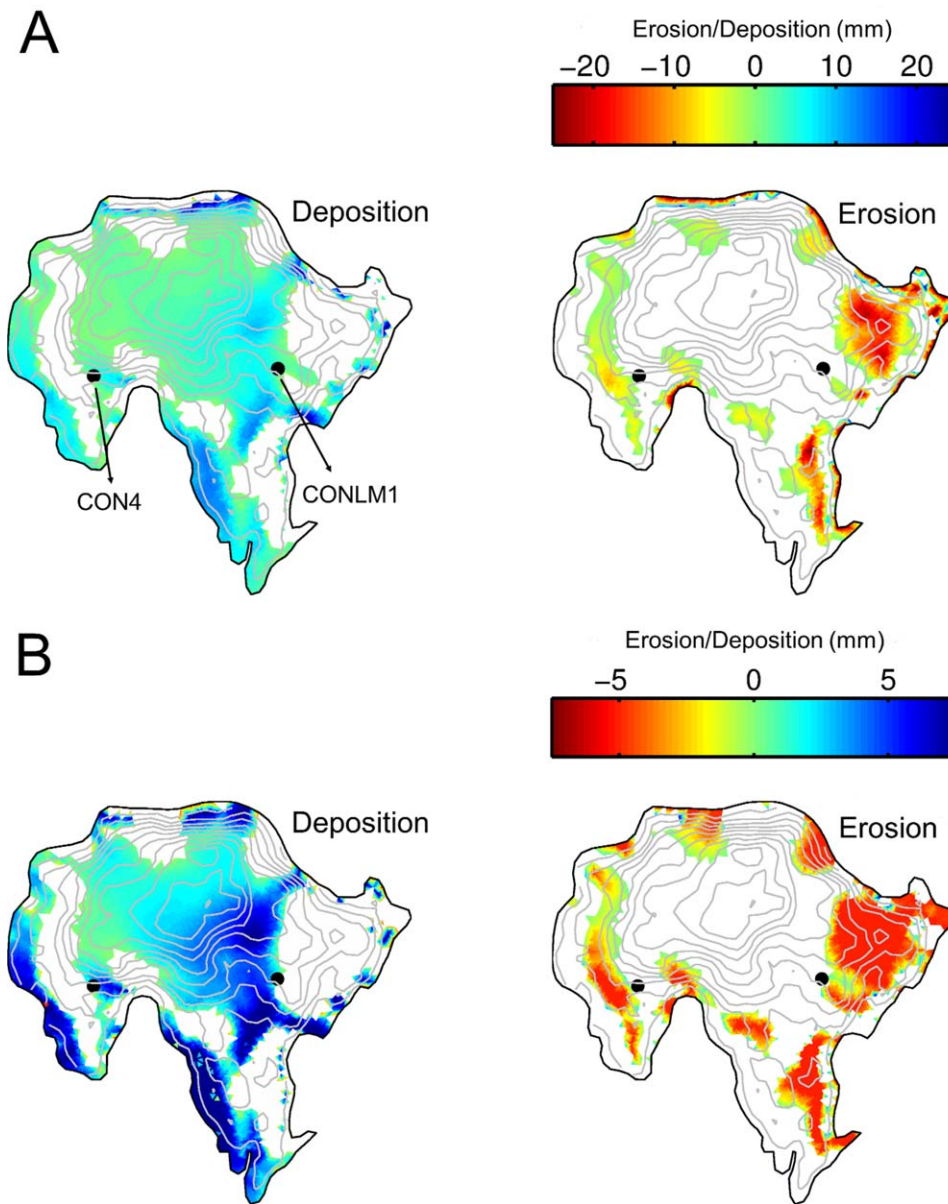


Fig. 5. Spatial patterns of deposition and erosion (cumulative bed elevation change over the 31-d run) for (A) run S1: unconstrained and (B) run S2: supply-limited. Locations of sediment cores CON4 and CONLM1 are indicated.

estimated suggests that this may be at least partly due to error in the wind forcing applied during the simulation, possibly the assumption of a uniform wind field.

Spatial pattern of erosion and deposition

Figure 5 shows simulated short-term bed evolution over the 31-d simulation period, disaggregated into regions of net deposition and erosion, for runs S1 and S2. In the transport-limited case, S1 (Fig. 5A), unlimited sediment supply from shallow areas subject to strong wave action drives sediment accumulation within the central part of the lake. The occurrence of winds and waves from all directions prevents

accumulation of muddy sediments around the entire shoreline. The combination of extremely high wind speeds and unlimited sediment supply accounts for unrealistically large rates of deposition—two orders of magnitude higher than recent historical rates inferred from the sediment cores (Fig. 4). Erosion is more localized, with “hotspots” along the northern and eastern shores where wave-generated bottom stresses are highest.

For the supply-limited scenario, S2 (Fig. 5B), lower absolute rates of change are obtained. However, the extreme wind forcing still drives deposition rates an order of magnitude greater than the long-term historic mean determined

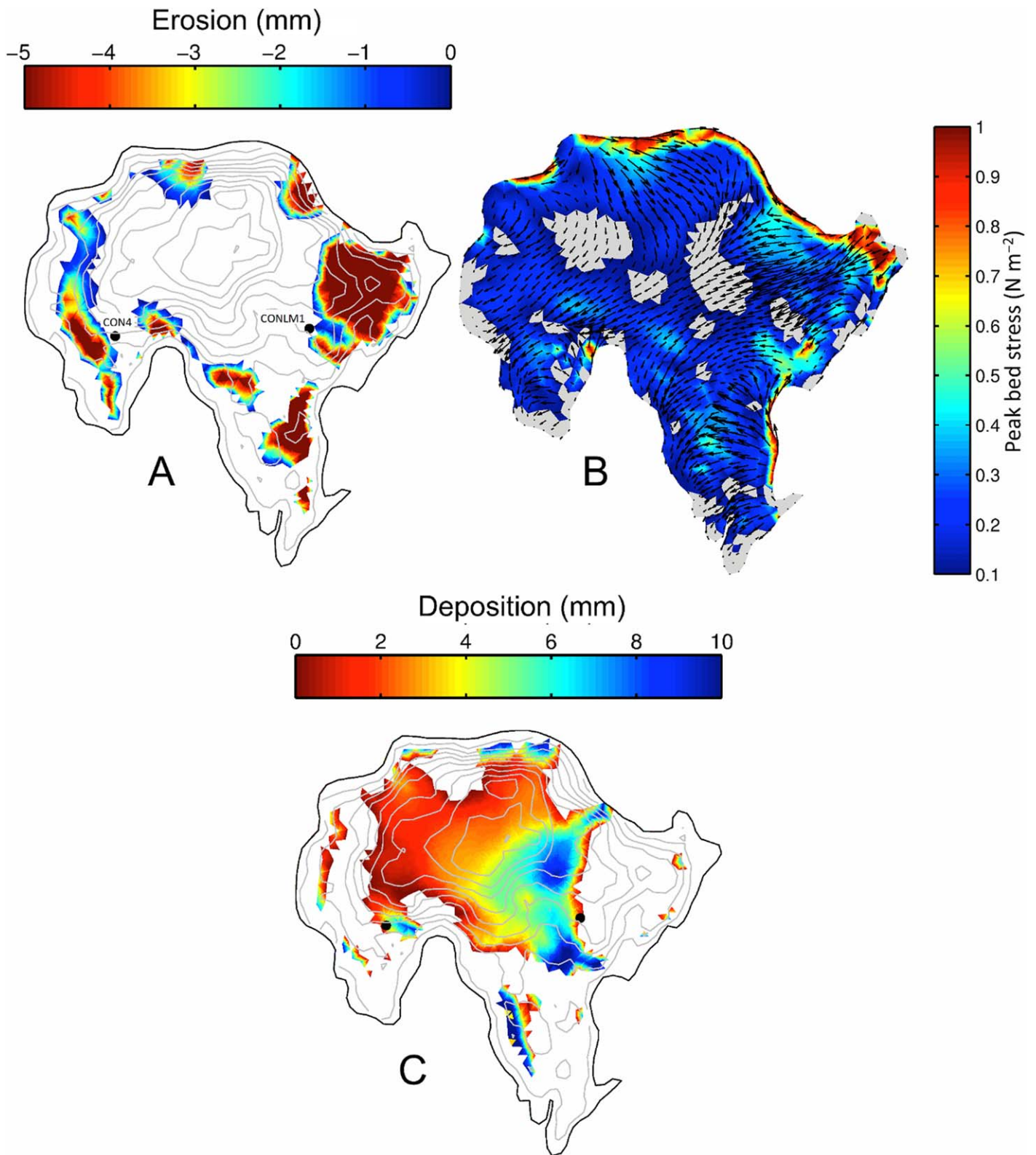


Fig. 6. (A) Spatial patterns of erosion for S2 supply-limited run, showing only those areas below the approximate wave base determined using the maximum wave height during the 31-d run; (B) maximum bottom shear stresses during S2 run with December 1997 forcing; (C) areas below wave base showing net deposition during run S2. Gray shaded areas correspond to $\tau_{\text{total}} < 0.1 \text{ N m}^2$. Vectors indicate the velocity field at the bottom.

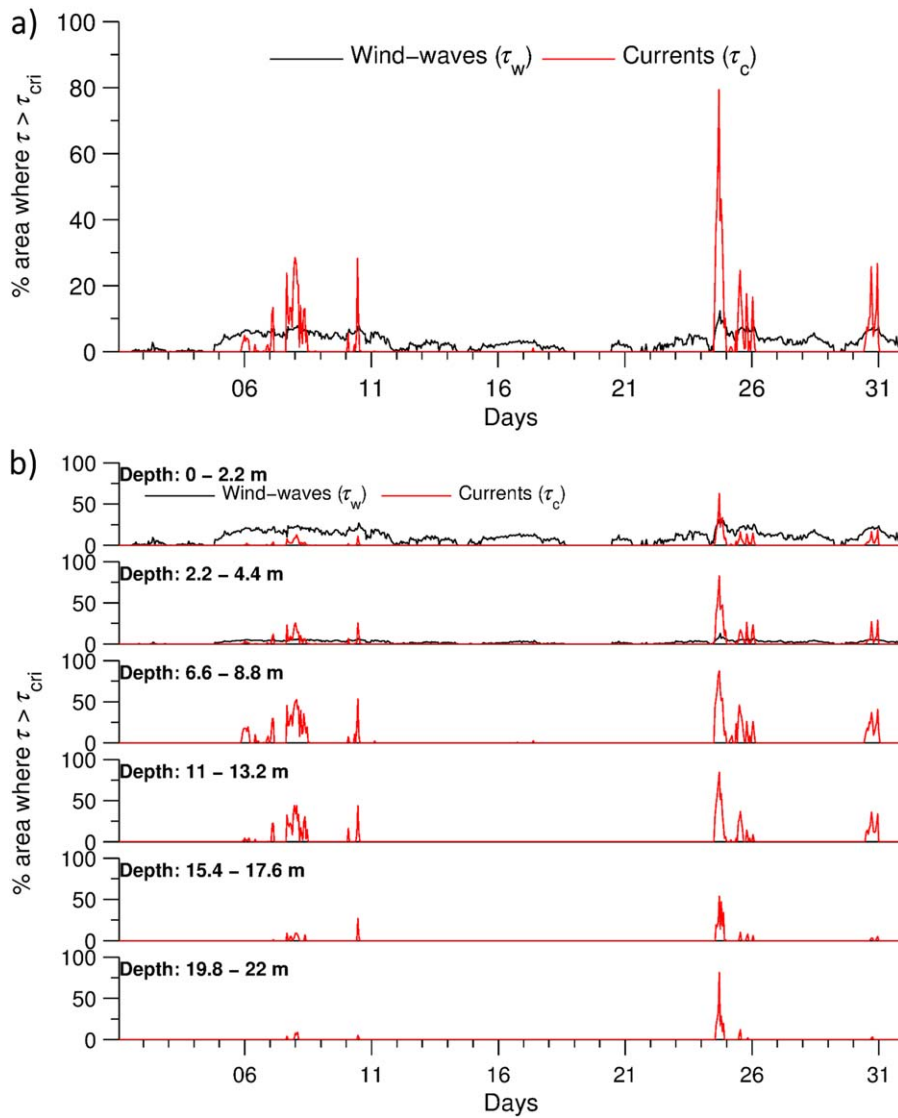


Fig. 7. (a) Time variation in lake-average bottom stress due waves and currents; (b) time-variation in wave and current bottom stress computed for selected depth ranges.

from Fig. 4. As expected, the supply constraint is especially evident in wave-eroded marginal source areas, although significant erosion extends into deeper water (> 10 m) within the eastern part of the basin; this area of net erosion is larger with the reduction in sediment supply from shallower water along the eastern margin of the lake. Foci of deposition occur in the lee of the small island (AWS location in Fig. 1) and several rock outcrops off the eastern shore that locally reduce wave energy. In reality, variability in the wind and wave direction precludes fine sediment accumulation in these areas. Overall spatial patterns of net erosion and deposition are broadly similar to those for S1.

Based on the computed wind wave characteristics, the maximum wave base lies at a depth of approximately 3.0 m. Widespread net erosion at depths below the wave base can

only be due to the currents and has implications for the efficacy of sediment focusing into deeper waters, the selection of locations for sediment coring, and the interpretation of sediment cores. Figure 6A shows the areas of the lake bed below the wave base that experience net erosion over the 31 d period of run S2. Figure 6B shows spatial variation in peak bottom stress over this period. It is interesting to note that sediment cores CON4 and CONLM1 both appear to lie just outside this erosional zone within the zones of net sediment deposition shown in Fig. 5. However, CONLM1 does lie within the zone where peak bottom stresses just exceed the critical bottom stress for erosion ($\tau_{cr} = 0.1 \text{ Nm}^{-2}$) used in run S2. This implies that deposition here is not 100% continuous and sediments may be reworked during extreme wind events. Clearly this finding depends to some extent on the

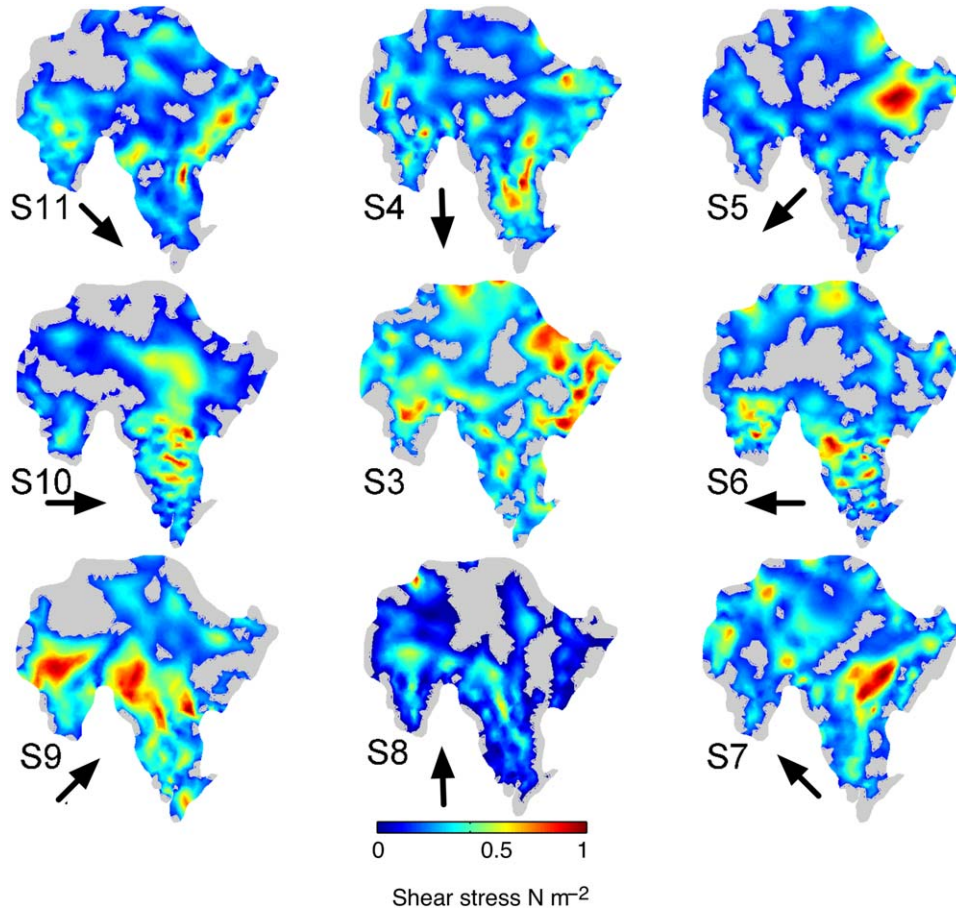


Fig. 8. Spatial distribution of bottom stress due to currents (wave model de-activated) under idealized constant wind direction scenarios (runs S4–S11), run S3 (variable wind direction) included in the center for comparison. See Table 1 for a summary of the model run parameters.

value of τ_{cr} and one should also acknowledge the positioning uncertainty in the core locations. But this does show the sensitivity of analyses of lake sediment sequences to the location of the cores, especially in small lakes such as this where gradients in topography, hydrodynamics, and sedimentation can be quite steep. Considering only the area below the wave base where net deposition occurs (Fig. 6C) it is also evident that the maximum deposition does not occur in the deepest part of the basin but on a plateau at intermediate depth. This is interpreted as a consequence of transport of sediment from the east due to the high bed stresses generated by the westward near-bed return flow of the wind-driven circulation. In the idealized simulations, this deposition is enhanced due to removal of the initial active layer from the shallower wave-dominated shelf to the west; actual deposition will likely be lower given that lake sediments are largely absent in the wave-dominated zone.

The relative importance of waves and currents as drivers of bed sediment dynamics varies over time and with depth. Figure 7a shows time-variation in the proportion of the lake bed that experiences $\tau_w > \tau_{crit} = 0.1 \text{ N m}^{-2}$ (waves) and

$\tau_c > \tau_{crit} = 0.1 \text{ N m}^{-2}$ (currents). At times of lower τ_w forcing, waves in the shallower areas are the dominant factor controlling sediment mobility at the bed. During the extreme wind events, a much larger proportion of the bed is potentially resuspended by currents. The partitioning of these processes by depth is shown in Fig. 7b. Waves cease to be effective in resuspending bottom sediments at depths greater than about 3 m. Resuspension in deeper water is solely due to currents but is much more intermittent.

It is interesting to consider spatial patterns of maximum current-generated bottom stresses for a set of idealized constant wind direction scenarios. Runs S3–S11 are forced by the same December 1997 wind speed time series, but apply constant wind directions in 45-degree bins (see Table 1 for summary). The sediment model is unchanged from run S2, except for the de-activation of the wave-generated bottom stresses. Figure 8 shows the distribution of $\tau_c > \tau_{crit} = 0.1 \text{ N m}^{-2}$ for each constant wind direction bin. Run S3 (in the center) shows the result using the actual (variable) wind directions and is a current-only re-run of S2. From S3, it is evident that currents alone can generate high bottom

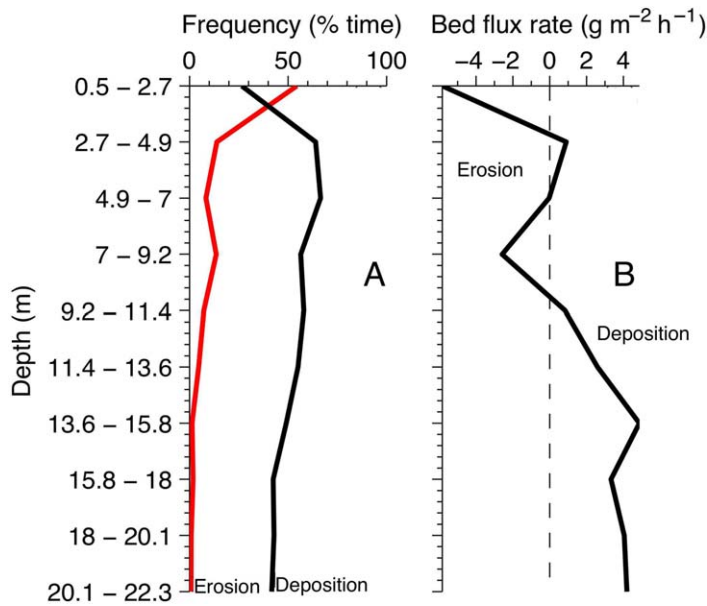


Fig. 9. (A) Frequency (% of the total time) of erosion and deposition vs. water depth. Note that frequencies do not sum to 100% because for some of the time the bottom stress is between the erosion and deposition thresholds used in the present simulations; (B) time- and space-averaged bed flux (erosion negative) vs. depth. [Color figure can be viewed at wileyonlinelibrary.com]

stresses in deeper water. While the highest current stresses occur in fairly shallow areas, $\tau_c > 0.5 \text{ N m}^{-2}$ (well above of any realistic value for τ_{crit}) occurs even in the deepest parts of the lake (water depth $> 20 \text{ m}$). The distribution of bottom stress is quite different for each of the fixed direction bins but, with the exception of southerly and easterly winds (run S8 and S6, respectively), zones of high maximum stress always occur in deep water. For the whole set of fixed direction runs (S4–S11), no part of the lake bed below the wave base is subject to maximum current stresses above 0.25 N m^{-2} .

Sediment focusing analysis

The ^{210}Pb chronologies for both the CON4 and CONLM1 cores (Supporting Information Table 2s; Fig. 4) imply a degree of sediment focusing in Llyn Conwy since the cumulative unsupported ^{210}Pb inventory exceeds the mean atmospheric flux for this region. However, both the distribution of deposits within the lake and the modeled sediment dynamics suggest that the mechanisms are more complex than envisaged in a simple focusing model. Crucially, the modeling predicts areas of net erosion well below the theoretical depth range of wind wave resuspension and even larger areas of intermittent sediment resuspension in deeper water.

An analysis of the relative temporal frequency of erosion and deposition in the various depth zones, averaged over the entire lake bed for model run S2, is presented in Fig. 9. The frequency of erosion decreases exponentially from the

shallowest waters ($h < 2.7 \text{ m}$) where erosion occurs $\sim 64\%$ of the time to the deepest areas, where it occurs less than 2.5% of the time. This is consistent with a negative (i.e., erosional) vertical bed flux in the shallow water zone and a positive (depositional) flux in deeper water. It also reflects the transition from regular wave-driven resuspension in shallow water to increasingly intermittent resuspension by currents in deeper water (see also Fig. 7). The most frequent deposition ($\sim 68\%$) occurs at intermediate water depths $4.9 \leq h < 7.0 \text{ m}$, and not at the deepest water, where deposition actually occurs less than 40% of the time. This finding can be explained by the fact that the deepest areas experience long periods during which current-generated bottom stresses exceed the deposition threshold while remaining below the erosion threshold. Such periods of effective bed stability are much less frequent in shallower water, since they depend on an absence of wave action and therefore calm weather conditions, which are unusual at this site.

Parameter sensitivity

Analysis of the various parameter sensitivity runs (Table 1) showed relatively little sensitivity to the values of d_{50} and w_s in terms of the spatial variation in net erosion and sedimentation and only a selection of the runs are summarized here (Fig. 10). For the range of sediment size and settling velocities used, the absolute bed level changes vary but the spatial patterns of change and the boundary between erosion and deposition are very similar. Variation in τ_{crit} clearly has a greater influence on the frequency with which wind-driven currents can mobilize lake bottom sediments. This is visualized in Fig. 11, which shows that resuspension is possible at depth even with an unrealistically high value of $\tau_{\text{crit}} = 0.2 \text{ N m}^{-2}$. Most of the simulations reported here use a fairly conservative value of $\tau_{\text{crit}} = 0.1 \text{ N m}^{-2}$; adoption of the possibly more realistic value of $\tau_{\text{crit}} = 0.05 \text{ N m}^{-2}$ significantly increases the prevalence of deep-water resuspension under strong wind forcing.

Discussion

Evaluation of alternative sediment focusing mechanisms

Not all of the four sediment focusing mechanisms identified by Hilton et al. (1986a) are relevant to Llyn Conwy. Given that this lake is oligotrophic, hosts virtually no aquatic macrophytes and has extremely low turbidity and nutrient loadings, the organic degradation mechanism can be readily discounted here.

The second factor, sliding and slumping, may be more significant. According to Håkanson (1977), sediment will not accumulate on slopes $> 14\%$. Below 4%, slope has no effect. A bottom slope map for Llyn Conwy (Fig. 12A) reveals a concentric zone around the deepest basin in which slopes exceed 10%. Slopes $< 5\%$ are found in the center of the basin, shallower areas along the western and eastern shores, and in the southern embayment. Shoreline slopes are

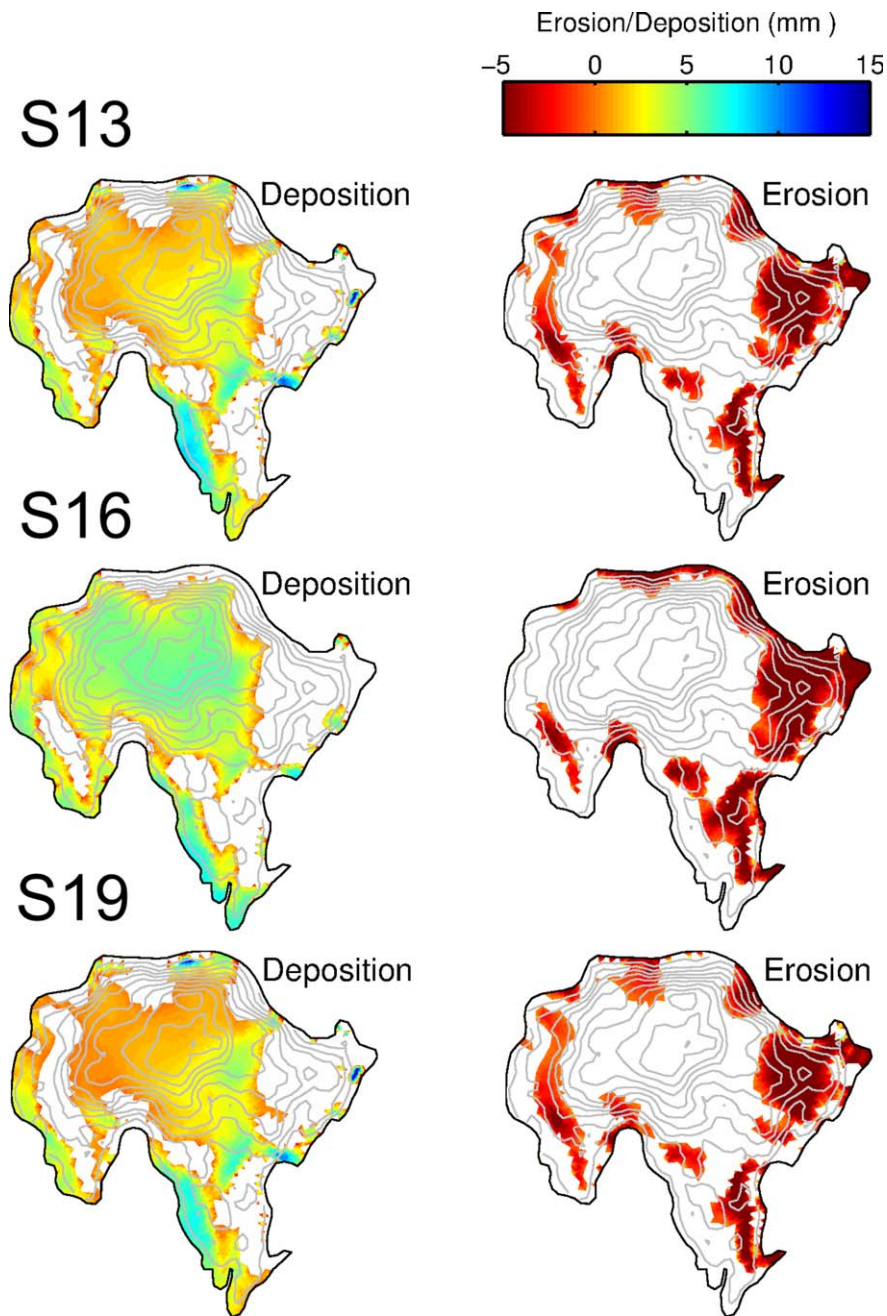


Fig. 10. Spatial patterns of deposition and erosion (cumulative bed elevation change over the 31-d run) for selected parameter sensitivity runs S13, S16, and S19 (variation in d_{50} and w_c). For parameter values see Table 1.

relatively consistent at around 7%, except in the north and northeast, where slopes are as steep as 23%.

Application of the Håkanson (1977) slope classification (Fig. 12B) shows that more than 70% of the bed is likely to accumulate sediments. The remaining 30% of the bed is conducive to sliding or by rotational failure, and focusing of sediments toward deeper water. Potential sediment pathways can be visualized by constructing a slope network (Fig. 12C).

Short paths across steeper slopes will likely be most effective in facilitating sliding of material into the deepest parts of the lake. Comparison of the slope zones with the observed distribution of bottom sediments (Fig. 3A) shows that steeper slopes along the northern margin are, as expected, free of lake sediments. However, the sediment deficient zone east of the central basin covers not only steeper slopes (e.g., A1 in Fig. 12A), but also a broad shelf (A2 in Fig. 12A). The western

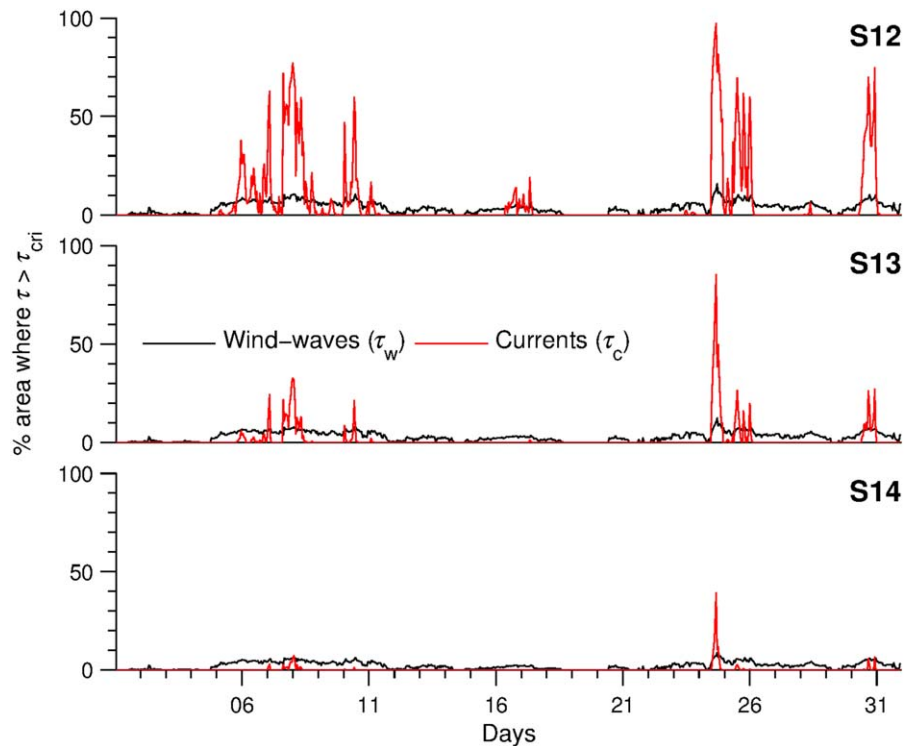


Fig. 11. Time variation in lake-average bottom stress due waves and currents for parameter sensitivity runs S12, S13, S14, showing the effect increasing critical stress for erosion ($\tau_{crit} = 0.05 \text{ Nm}^{-2}$, 0.1 Nm^{-2} , and 0.2 Nm^{-2} , respectively).

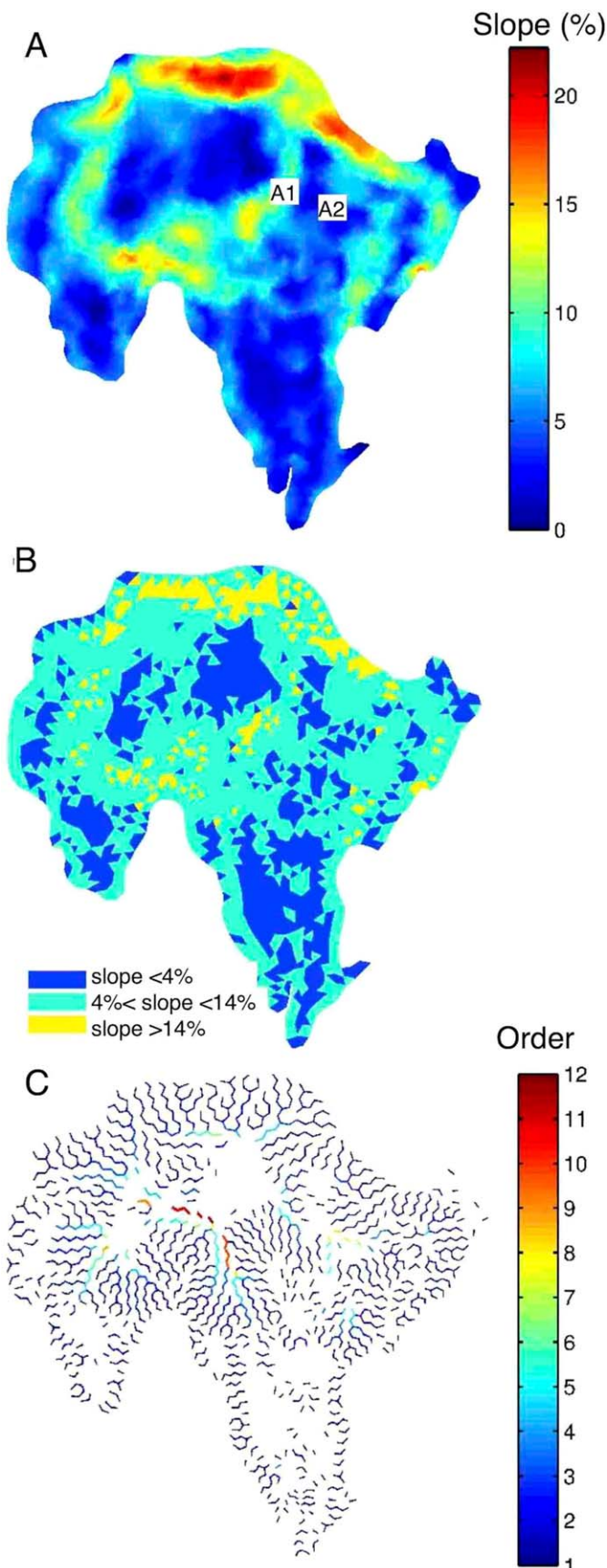
margins of the basin appear to be mantled with sediment despite extensive areas of intermediate gradient and localized slopes $> 14\%$. Slope is certainly a potential factor controlling sedimentation in Llyn Conwy and may be responsible for disturbances to the sediment sequence (e.g., by slope failures) that sparse grab sampling and coring cannot resolve. An early application of seismic stratigraphic survey by Cronin et al. (1993) to another small upland lake in Wales found limited evidence for slumping of highly organic sediments on slopes of about 15 degrees (26%) and it would be interesting to undertake bed imaging (e.g., using sidescan sonar) in Llyn Conwy to investigate the prevalence of slides and slumps.

Hilton et al. (1986a) also describe a process that they term “intermittent complete mixing,” driven by widespread resuspension, mixing, and settling. This leads to sediment focusing by virtue of the greater water column sediment mass in deeper water. The exposure of Llyn Conwy to strong south-westerly winds, leads to persistent overturn during winter and autumn, and intermittent but frequent mixing in summer. Such behavior is only possible in smaller lakes, and the rapid breakdown of the thermocline is one factor that allows resuspension of sediment in deeper water. As the exploratory modeling presented here shows, the wind-driven circulation can be quite complex and high bottom stresses can be generated by currents in the deepest parts of a lake.

In the case of Llyn Conwy, this means that a large proportion of the lake bed experiences resuspension of sediments at least some of the time (Fig. 7).

The fourth mechanism, peripheral wave action is clearly important in Llyn Conwy. Despite the limited fetch, significant wave heights of 0.3 m commonly occur, with heights up to 0.8 m along the northern and eastern shores in the December 1997 simulations. This precludes sediment accumulation, such that the shores are dominated by coarse lag deposits. Our exploratory modeling shows that wave-generated bed stresses are typically an order of magnitude greater than those due to currents in shallow water areas. The wave base (and therefore the mud deposition boundary) is approximated by the 3 m depth contour in the most exposed locations. Sediment resuspended by waves is efficiently transported out to deeper water, where settling occurs. In Esthwaite Water, Hilton et al. (1986a) found that 6% of the total variance of the accumulation rate estimated by sediment traps was due to wave action, manifest as a negative correlation between sedimentation rate and fetch. Similar studies of lakes in the Muskoba-Haliburton region of Canada (Hilton 1985) also implicate peripheral wave action, in conjunction with intermittent complete mixing, as the main mechanisms of sediment focusing.

The above analysis suggests that three of the four mechanisms that Hilton et al. (1986a) associate with sediment



focusing are potentially important in Llyn Conwy and possibly within oligotrophic upland lakes in general. Intermittent complete mixing and peripheral wave action appear to be the most important based upon the observations and modeling presented here.

Implications for environmental reconstruction based on lake sediment cores

Reconstruction of environmental change from lake sediment sequences depends on the acquisition and analysis of core samples from sites of continuous sediment accumulation (Håkanson and Jansson 1983). The basic sediment focusing model (Lehman 1975; Blais and Kalff 1995) provides one means of, a priori, selecting suitable locations based on bathymetric data alone. Such work has been extended in two main directions. First, various workers have attempted to improve the statistical basis for sampling by considering the number of cores necessary to provide an acceptable level of precision in the estimation of whole lake sedimentation rates (e.g., Håkanson 1984; Baudo et al. 1989; Floderus 1989). Second, efforts have been made to improve the dynamic basis of the sediment focusing model. These have mostly involved modeling of wave-driven redistribution of sediment from shallow to deeper water (e.g., Sheng and Lick 1979; Bengtsson and Hellström 1992; Löfstedt and Bengtsson 2008). Rowan et al. (1992) quantified the mud deposition boundary depth and used this to determine the locate and optimize the number of cores needed to estimate mean sedimentation rates (Rowan et al. 1995). More recently, Mackay et al. (2012) examined the effects of wind-waves, currents and bed slopes and wind-induced currents, on sediment redistribution and argued that the heterogeneity of carbon and phosphorus deposition patterns in small lakes is largely due to such factors.

Our study of Llyn Conwy reveals a patchy distribution of lake sediments even within these deeper waters that is controlled not only by wave-driven transfer from shallow to deep water and by redistribution down-slope, but also by wind-driven currents. Exploratory numerical modeling also shows that near-bed currents are able to generate bottom stresses in excess of plausible critical stresses for erosion. Although areas with no sedimentation account for a fairly small proportion of the lake bed, currents are clearly capable of intermittently re-suspending deep water sediments, disturbing otherwise continuous depositional sequences. A priori prediction of these zones is difficult since the wind-driven circulation is governed by complex non-linear interactions between meteorological forcing and lake geometry. These can only be understood and predicted through physically based modeling of the kind reported here.

Fig. 12. Summary analysis of Llyn Conwy bottom slope: (A) spatial variation in bottom slope; (B) bottom slope classified according to Håkanson (1977) scheme; (C) downslope pathways for slopes > 4.

Conclusions

This study has used a three-dimensional numerical hydrodynamic and suspended sediment model in combination with a semi-empirical wind wave model to investigate the extent to which sedimentation accumulation in upland lakes is controlled by focusing of sediments toward a deep-water sink. Exploratory simulations of wave- and current-generated bottom stress and suspended sediment dynamics in a small oligotrophic upland lake confirm the expected importance of peripheral wave action as a sediment focusing mechanism. In deeper water, wind-driven currents become the dominant contributor to bottom stress. Strong wind forcing drives an energetic circulation with peak bottom stresses that intermittently exceed any realistic erosion threshold over a most of the lake bed at depths far below those at which waves can be effective. The spatial distribution of lake sediments, and the completeness of the sediment record, is thus determined by a complex interaction between wind-driven circulation and bathymetry, rather than by continuous accumulation in the deepest part of the basin. Although our sediment dynamics simulations are purely exploratory, the results are consistent with survey results that show a patchy distribution of deep-water accumulation.

These findings have implications for palaeolimnological studies, which often rely on the acquisition of cores from the deepest location of a lake on the assumption that sedimentation here is relatively rapid and also continuous. Given that bathymetric and meteorological data are often available, hydrodynamic modeling of the wind-driven circulation should be more widely used to refine selection of coring locations and also to determine the likely frequency and extent of sediment reworking and its effect on the various palaeoenvironmental proxies of interest.

References

- Appleby, P., P. Nolan, D. Gifford, M. Godfrey, F. Oldfield, N. Anderson, and R. Battarbee. 1986. ^{210}Pb dating by low background gamma counting. *Hydrobiologia* **143**: 21–27. doi:10.1007/BF00026640
- Appleby, P., N. Richardson, and P. Nolan. 1991. ^{241}Am dating of lake sediments. *Hydrobiologia* **214**: 35–42. doi:10.1007/BF00050929
- Appleby, P., N. Richardson, and P. Nolan. 1992. Self-absorption corrections for well-type germanium detectors. *Nucl. Instrum. Methods* **71**: 228–233. doi:10.1016/0168-583X(92)95328-O
- Austnes, K., C. Evans, C. Eliot-Laze, P. Naden, and G. Old. 2010. Effects of storm events on mobilisation and in-stream processing of dissolved organic matter (DOM) in a Welsh peatland catchment. *Biogeochemistry* **99**: 157–173. doi:10.1007/s10533-009-9399-4
- Battarbee, R. W. 1978. Observations on the recent history of Lough Neagh and its drainage basin. *Philos. Trans. R. Soc. B* **281**: 303–345. doi:10.1098/rstb.1978.0001
- Battarbee, R. W. 2000. Palaeolimnological approaches to climate change, with special regard to the biological record. *Quat. Sci. Rev.* **19**: 107–124. doi:10.1016/S0277-3791(99)00057-8
- Baudo, R., L. Amantini, F. Bo, R. Cenci, P. Hannaert, A. Lattanzio, G. Marengo, and H. Muntau. 1989. Spatial distribution patterns of metals in the surface sediments of Lake Orta (Italy). *Sci. Total Environ.* **87**: 117–128. doi:10.1016/0048-9697(89)90229-5
- Bengtsson, L., and T. Hellström. 1992. Wind-induced resuspension in a small shallow lake. *Hydrobiologia* **241**: 163–172. doi:10.1007/BF00028639
- Blais, J., and J. Kalff. 1995. The influence of lake morphometry on sediment focusing. *Limnol. Oceanogr.* **40**: 582–588. doi:10.4319/lo.1995.40.3.0582
- Blom, G., E. Duin, R. Aalderink, L. Lijklema, and C. Toet. 1992. Modelling sediment transport in shallow lakes - interactions between sediment transport and sediment composition. *Hydrobiologia* **235**: 153–166. doi:10.1007/BF00026208
- Booij, N., R. Ris, and L. Holthuijsen. 1999. A third-generation wave model for coastal regions. I-Model description and validation. *J. Geophys. Res.* **104**: 7649–7666. doi:10.1029/98JC02622
- Brothers, S., J. Vermaire, and I. Gregory-Eaves. 2008. Empirical models for describing recent sedimentation rates in lakes distributed across broad spatial scales. *J. Paleolimnol.* **40**: 1003–1019. doi:10.1007/s10933-008-9212-8
- Cea, L., and J. R. French. 2012. Bathymetric error estimation for the calibration and validation of estuarine hydrodynamic models. *Estuar. Coast. Shelf Sci.* **100**: 124–132. doi:10.1016/j.ecss.2012.01.004
- CERC. 1984. Shore protection manual. U.S. Army Corps of Engineers, Coastal Engineering Research Center, Vicksburg.
- Chambers, J., and N. Cameron. 2001. A rod-less piston corer for lake sediments; an improved, rope-operated percussion corer. *J. Paleolimnol.* **25**: 117–122. doi:10.1023/A:1008181406301
- Chao, X., Y. Jia, F. Shields, S. Wang, and C. Cooper. 2008. Three-dimensional numerical modeling of cohesive sediment transport and wind wave impact in a shallow oxbow lake. *Adv. Water Resour.* **31**: 1004–1014. doi:10.1016/j.advwatres.2008.04.005
- Chen, C., and others. 2004. Impacts of suspended sediment on the ecosystem in Lake Michigan: A comparison between the 1998 and 1999 plume events. *J. Geophys. Res.* **109**. C10S05, doi:10.1029/2002JC001687
- Chen, C., G. Cowles, and R. Beardsley. 2011. An unstructured grid, finite-volume community ocean model: FVCOM user manual, p. 315, 3rd ed. Univ. of Massachusetts-Dartmouth.
- Cronin, S., H. Lamb, and R. Whittington. 1993. Seismic reflection and sonar survey as a aid to the investigation of lake sediment stratigraphy: A case study from upland wales, p. 181–203. *In* J. McManus and R. Duck [eds.],

- Geomorphology and sedimentology of lakes and reservoirs. Wiley.
- Cyr, H. 1998. Effects of wave disturbance and substrate slope on sediment characteristics in the littoral zone of small lakes. *Can. J. Fish. Aquat. Sci.* **55**: 967–976. doi:10.1139/f97-298
- Davis, M. 1969. Climatic changes in southern Connecticut recorded by pollen deposition at Rogers Lake. *Ecology* **50**: 409–422. doi:10.2307/1933891
- Davis, M., and M. Ford. 1982. Sediment focusing in Mirror Lake, New Hampshire. *Limnol. Oceanogr.* **27**: 137–150. doi:10.4319/lo.1982.27.1.0137
- Dearing, J. 1986. Core correlation and total sediment influx, p. 247–270. *In* B. E. Berglund [ed.], *Handbook of palaeoecology and palaeohydrology*. Wiley.
- Dyer, K. 1986. *Coastal and estuarine sediment dynamics*. Wiley.
- Evans, R. 1994. Empirical evidence of the importance of sediment resuspension in lakes. *Hydrobiologia* **284**: 5–12. doi:10.1007/BF00005727
- Floderus, S. 1989. Sediment sampling evaluated with a new weighting function and index of reliability. *Hydrobiologia* **176**: 451–464. doi:10.1007/BF00026581
- Folk, R., and W. Ward. 1957. Brazos river bar: A study in the significance of grain size parameters. *J. Sediment. Petrol.* **27**: 3–26. doi:10.1306/74D70646-2B21-11D7-8648000102C1865D
- Foster, I., J. Dearing, and R. Grew. 1988. Lake-catchments: A evaluation of their contribution to studies of sediment yield and delivery processes, p. 413–424. IAHS Public 174.
- Fritz, S. 1996. Paleolimnological records of climatic change in North America. *Limnol. Oceanogr.* **41**: 882–889. doi:10.4319/lo.1996.41.5.0882
- Gajewski, K., P. Hamilton, and R. McNeely. 1997. A high resolution proxy-climate record from an arctic lake with annually-laminated sediments on Devon Island, Nunavut, Canada. *J. Paleolimnol.* **17**: 215–225. doi:10.1023/A:1007984617675
- Galperin, B., L. Kantha, S. Hassid, and A. Rosati. 1988. A quasi-equilibrium turbulent energy model for geophysical flows. *J. Atmos. Sci.* **45**: 55–62. doi:10.1175/1520-0469(1988)045<0055:AQETEM>2.0.CO;2
- Gilbert, R. 2003. Spatially irregular sedimentation in a small, morphologically complex lake: Implications for paleoenvironmental studies. *J. Paleolimnol.* **29**: 209–220. doi:10.1023/A:1023287009148
- Gloor, M., A. Wüest, and M. Münnich. 1994. Benthic boundary mixing and resuspension induced by internal seiches. *Hydrobiologia* **284**: 59–68. doi:10.1007/BF00005731
- Håkanson, L. 1977. The influence of wind, fetch, and water depth on the distribution of sediments in Lake Vänern, Sweden. *Can. J. Earth Sci.* **14**: 397–412. doi:10.1139/e77-040
- Håkanson, L. 1981. *A manual of lake morphometry*. Springer-Verlag.
- Håkanson, L. 1984. On the relationship between lake trophic level and lake sediments. *Water Res.* **18**: 303–314. doi:10.1016/0043-1354(84)90104-0
- Håkanson, L., and M. Jansson. 1983. *Principles of lake sedimentology*. Springer.
- Harris, C., and P. Wiberg. 1997. Approaches to quantifying long-term continental shelf sediment transport with an example from the Northern California STRESS mid-shelf site. *Cont. Shelf Res.* **17**: 1389–1418. doi:10.1016/S0278-4343(97)00017-4
- Hilton, J. 1985. A conceptual framework for predicting the occurrence of sediment focusing and sediment redistribution in small lakes. *Limnol. Oceanogr.* **30**: 1131–1143. doi:10.4319/lo.1985.30.6.1131
- Hilton, J., J. Lishman, and P. Allen. 1986a. The dominant processes of sediment distribution and focusing in a small, eutrophic, monomictic lake. *Limnol. Oceanogr.* **31**: 125–133. doi:10.4319/lo.1986.31.1.0125
- Hilton, J., J. Lishman, and A. Millington. 1986b. A comparison of some rapid techniques for the measurement of density in soft sediments. *Sedimentology* **33**: 777–781. doi:10.1111/j.1365-3091.1986.tb01976.x
- Imberger, J. 1998. *Physical processes in lakes and oceans*. American Geophysical Union.
- Itkonen, A., and V. Salonen. 1994. The response of sedimentation in three varved lacustrine sequences to air temperature, precipitation and human impact. *J. Paleolimnol.* **11**: 323–332. doi:10.1007/BF00677992
- Ji, Z. [ed.]. 2008. *Hydrodynamics and water quality: Modeling rivers, lakes, and estuaries*. Wiley.
- Kazancı, N., and others. 2010. Wind control on the accumulation of heavy metals in sediment of Lake Ulubat, Anatolia, Turkey. *J. Paleolimnol.* **43**: 89–110. doi:10.1007/s10933-009-9316-9
- Larsen, C., and G. MacDonald. 1993. Lake morphometry, sediment mixing and the selection of field sites for fine resolution palaeoecological studies. *Quat. Sci. Rev.* **12**: 781–792. doi:10.1016/0277-3791(93)90017-G
- Lee, D.-Y., and H. Wang. 1984. Measurement of surface waves from subsurface gage, p. 271–286. *In* Proceedings of 19th International Conference on Coastal Engineering, vol. **1**. Houston, Texas.
- Leeder, M. 1982. *Sedimentology*. Allen & Unwin.
- Lehman, J. 1975. Reconstructing the rate of accumulation of lake sediment: The effect of sediment focusing. *Quat. Res.* **5**: 1–550. doi:10.1016/0033-5894(75)90015-0
- Likens, G., and M. Davis. 1975. Post-glacial history of Mirror Lake and its watershed in New Hampshire, USA: An initial report. *Int. Ver. Theor. Angew. Limnol. Verh.* **19**: 982–993.
- Lou, J., D. Schwab, D. Beletsky, and N. Hawley. 2000. A model of sediment resuspension and transport dynamics in southern Lake Michigan. *J. Geophys. Res.* **105**: 6591–6610. doi:10.1029/1999JC900325

- Lövstedt, C., and L. Bengtsson. 2008. The role of non-prevailing wind direction on resuspension and redistribution of sediments in a shallow lake. *Aquat. Sci.* **70**: 304–313. doi:10.1007/s00027-008-8047-8
- Luettich, R., D. Harleman, and L. Somlyódy. 1990. Dynamic behavior of suspended sediment concentrations in a shallow lake perturbed by episodic wind events. *Limnol. Oceanogr.* **35**: 1050–1067. doi:10.4319/lo.1990.35.5.1050
- Mackay, E., I. Jones, A. Folkard, and P. Barker. 2012. Contribution of sediment focussing to heterogeneity of organic carbon and phosphorus burial in small lakes. *Freshw. Biol.* **57**: 290–304. doi:10.1111/j.1365-2427.2011.02616.x
- Margalef, R. 1983. *Limnología*. Omega.
- Mellor, G., and T. Yamada. 1982. Development of a turbulence closure model for geophysical fluid problems. *Rev. Geophys.* **20**: 851–875. doi:10.1029/RG020i004p00851
- Morales-Marín, L. A. 2013. Numerical modelling of hydrodynamics and sedimentation in upland lakes: A test of the sediment focusing hypothesis. Ph.D. thesis. Univ. College London.
- Nash, J., and J. Sutcliffe. 1970. River flow forecasting through conceptual models part I – a discussion of principles. *J. Hydrol.* **10**: 282–290. doi:10.1016/0022-1694(70)90255-6
- Odgaard, B. V. 1993. Wind-determined sediment distribution and Holocene sediment yield in a small, Danish, kettle lake. *J. Paleolimnol.* **8**: 3–13. doi:10.1007/BF00210054
- O’Sullivan, P. 1983. Annually-laminated lake sediments and the study of Quaternary environmental changes—a review. *Quat. Sci. Rev.* **1**: 245–313. doi:10.1016/0277-3791(83)90008-2
- Patrick, S., and A. Stevenson. 1986. Palaeoecological evaluation of the recent acidification of Welsh lakes Part 3; Llyn Conwy and Gamallt, Gwynedd. Tech. Rep. 19, Palaeoecology Research Unit, Univ. College London.
- Reading, H. G., and J. D. Collinson. 1996. Clastic coasts, p. 154–258. *In* H. G. Reading [ed.], *Sedimentary environments: Processes, facies and stratigraphy*. Blackwell Science.
- Rowan, D., J. Kalf, and J. Rasmussen. 1992. Estimating the mud deposition boundary depth in lakes from wave theory. *Can. J. Fish. Aquat. Sci.* **4**: 2490–2497. doi:10.1139/f92-275
- Rowan, D., R. Cornett, K. King, and B. Risto. 1995. Sediment focusing and ²¹⁰Pb dating: A new approach. *J. Paleolimnol.* **13**: 107–118. doi:10.1007/BF00678101
- Sheng, Y., and W. Lick. 1979. The transport and resuspension of sediments in a shallow lake. *J. Geophys. Res.* **84**: 1809–1826. doi:10.1029/JC084iC04p01809
- Smagorinsky, J. 1963. General circulation experiments with the primitive equations. *Mon. Weather Rev.* **91**: 99–164. doi:10.1175/1520-0493(1963)091 <0099:GCEWTP>2.3.CO;2
- Smith, I. 1979. Hydraulic conditions in isothermal lakes. *Freshw. Biol.* **9**: 119–145. doi:10.1111/j.1365-2427.1979.tb01496.x
- Smol, J. 1992. Paleolimnology: An important tool for effective ecosystem management. *J. Aquat. Ecosyst. Stress Recover.* **1**: 49–58. doi:10.1007/BF00044408
- Solovieva, N., and others. 2005. Palaeolimnological evidence for recent climatic change in lakes from the northern Urals, arctic Russia. *J. Paleolimnol.* **33**: 463–482. doi:10.1007/s10933-005-0811-3
- Stern, G., and others. 2005. Modern and historical fluxes of halogenated organic contaminants to a lake in the Canadian arctic, as determined from annually laminated sediment cores. *Sci. Total Environ.* **342**: 223–243. doi:10.1016/j.scitotenv.2004.12.046
- Stumm, W. 1985. *Chemical processes in lakes*. Wiley.
- Trenberth, K. E. 1989. The effective drag coefficient for evaluating wind stress over the oceans. *J. Clim.* **2**: 1507–1516. doi:10.1175/1520-0442(1989)002 <1507:TEDCFE>2.0.CO;2
- Verschuren, D. 1999. Sedimentation controls on the preservation and time resolution of climate-proxy records from shallow fluctuating lakes. *Quat. Sci. Rev.* **18**: 821–837. doi:10.1016/S0277-3791(98)00065-1
- Wang, H., J. Holmes, F. Street-Perrott, M. Waller, and R. Perrott. 2008. Holocene environmental change in the West African Sahel: Sedimentological and mineral-magnetic analyses of lake sediments from Jikariya Lake, northeastern Nigeria. *J. Quat. Sci.* **23**: 449–460. doi:10.1002/jqs.1154
- Warner, J., C. Sherwood, R. Signell, C. Harris, and H. Arango. 2008. Development of a three-dimensional, regional, coupled wave, current, and sediment-transport model. *Comput. Geosci.* **34**: 1284–1306. doi:10.1016/j.cageo.2008.02.012
- Yelland, M., and P. K. Taylor. 1996. Wind stress measurements from the open ocean. *J. Phys. Oceanogr.* **26**: 541–558. doi:10.1175/1520-0485(1996)026 <0541:WSMFTO>2.0.CO;2
- Young, I., and L. Verhagen. 1996. The growth of fetch limited waves in water of finite depth. Part 1. Total energy and peak frequency. *Coast. Eng.* **29**: 47–78. doi:10.1016/S0378-3839(96)00006-3

Acknowledgments

Luis A. Morales-Marín acknowledges financial support from UCL Department of Geography in the form of a Postgraduate Computing Assistantship. The project was also partly supported by NERC award NE/I007520/1 (UKLEON). We thank Ian Patmore for his sterling assistance with the boat work, sediment coring and instrument deployments at Llyn Conwy. Dr Handong Yang in the UCL Bloomsbury Environmental Isotope Facility undertook the analysis of sediment core CONLM1. We also acknowledge provision of UK Meteorological Office MIDAS Land Surface Observations data via the British Atmospheric Data Centre and thank the Centre of Ecology and Hydrology (CEH) at Bangor for allowing access to 2006–2008 AWS data for Llyn Conwy.

Conflict of Interest

None declared.

Submitted 22 August 2016

Revised 04 July 2017

Accepted 05 September 2017

Associate editor: Francisco Rueda